The Plant Cell, Vol. 30: 1023–1039, May 2018, www.plantcell.org © 2018 ASPB.

Phosphatidic Acid Counteracts S-RNase Signaling in Pollen by Stabilizing the Actin Cytoskeleton

Jianqing Chen,[a,b] Peng Wang,[a] Barend H.J. de Graaf,[c] Hao Zhang,[a] Huijun Jiao,[a] Chao Tang,[a] Shaoling Zhang,[a,1] and Juyou Wu[a,1]

[a] Center of Pear Engineering Technology Research, State Key Laboratory of Crop Genetics and Germplasm Enhancement, College of Horticulture, Nanjing Agricultural University, Nanjing 210095, China
[b] College of Horticulture, Fujian Agriculture and Forestry University, Fuzhou 350002, China
[c] School of Biosciences, Cardiff University, Museum Avenue, Cardiff CF10 3AX, United Kingdom

ORCID IDs: 0000-0002-7521-5925 (P.W.); 0000-0003-0542-5510 (B.H.d.G.); 0000-0001-7479-151X (J.W.)

S-RNase is the female determinant of self-incompatibility (SI) in pear (*Pyrus bretschneideri*). After translocation to the pollen tube, S-RNase degrades rRNA and induces pollen tube death in an *S*-haplotype-specific manner. In this study, we found that the actin cytoskeleton is a target of *P. bretschneideri* S-RNase (PbrS-RNase) and uncovered a mechanism that involves phosphatidic acid (PA) and protects the pollen tube from PbrS-RNase cytotoxicity. PbrS-RNase interacts directly with PbrActin1 in an *S*-haplotype-independent manner, causing the actin cytoskeleton to depolymerize and promoting programmed cell death in the self-incompatible pollen tube. Pro-156 of PbrS-RNase is essential for the PbrS-RNase-PbrActin1 interaction, and the actin cytoskeleton-depolymerizing function of PbrS-RNase does not require its RNase activity. PbrS-RNase cytotoxicity enhances the expression of phospholipase D (PbrPLDδ1), resulting in increased PA levels in the incompatible pollen tube. PbrPLDδ1-derived PA initially prevents depolymerization of the actin cytoskeleton elicited by PbrS-RNase and delays the SI signaling that leads to pollen tube death. This work provides insights into the orchestration of the S-RNase-based SI response, in which increased PA levels initially play a protective role in incompatible pollen, until sustained PbrS-RNase activity reaches the point of no return and pollen tube growth ceases.

INTRODUCTION

The success of sexual reproduction in flowering plants, which results in the production of seeds to secure the next generation, is entirely dependent on species-specific communication between pollen and the pistil. After pollination, the pollen grain germinates and produces a tube that delivers nonmotile sperm cells to the ovary for fertilization. To achieve this, pollen tubes usually grow over relatively long distances through the pistil to reach the base, where the ovules with egg cells are located (Higashiyama and Takeuchi, 2015). However, within a given species, the presence of genetically determined barriers, i.e., a mechanism known as self-incompatibility (SI), may prevent self-fertilization in order to promote outbreeding (De Nettancourt, 2001; Franklin-Tong, 2008; Doucet et al., 2016; Fujii et al., 2016). SI is genetically controlled by a highly polymorphic *S*-locus that harbors two physically linked *S*-genes. SI allows the pistil of a plant to reject only pollen originating from the same plant or pollen from a neighboring plant that carries the same SI genotype (De Nettancourt, 2001; Franklin-Tong, 2008).

The most widespread form of SI operates through a pistil-expressed S-RNase mechanism, which has been intensively studied in the Solanaceae, Plantaginaceae, and Rosaceae families (Anderson et al., 1986; Sassa et al., 1992; Xue et al., 1996). In S-RNase-based SI, the female determinant encodes an S-RNase, whereas the male determinant encodes an S-locus F-box protein. Following pollination and pollen germination, S-RNases are translocated to the growing pollen tube, where the activity of incompatible S-RNases eventually leads to the failsafe arrest of growth of incompatible pollen tubes.

S-RNases belong to the RNase T2 family, which is widely represented in prokaryotes and eukaryotes. Members of this family have a wide range of cytotoxic functions, from degrading rRNA to inducing cell death (Luhtala and Parker, 2010). S-RNases are specifically expressed in transmitting tissue cells of the pistil and are secreted into the intercellular matrix, the pathway for pollen tube growth. After pollination, regardless of the pollen (n) and pistil (2n) *S*-haplotypes, both S-RNases enter the growing pollen tube (Luu et al., 2000; Meng et al., 2014). In compatible pollen tubes, non-self S-RNases are degraded by the ubiquitin 26S proteasome (Lai et al., 2002; Qiao et al., 2004; Sijacic et al., 2004) or are compartmentalized into the vacuole (Goldraij et al., 2006). However, in incompatible pollen tubes, self S-RNases are protected from degradation and have a cytotoxic effect; this inhibits pollen tube growth and results in pollen tube death, thus preventing the delivery of sperm cells to the ovules.

Several downstream signaling factors that function in incompatible pollen have been identified and shown to be essential for the success of S-RNase-based SI. For example, in pear (*Pyrus bretschneideri*), a fruit tree of the Rosaceae family, we found that

[1] Address correspondence to juyouwu@njau.edu.cn or slzhang@njau.edu.cn.
The authors responsible for distribution of materials integral to the findings presented in this article in accordance with the policy described in the Instructions for Authors (www.plantcell.org) are: Juyou Wu (juyouwu@njau.edu.cn) and Shaoling Zhang (slzhang@njau.edu.cn).
www.plantcell.org/cgi/doi/10.1105/tpc.18.00021

IN A NUTSHELL

Background: The success of sexual reproduction in flowering plants is entirely dependent on communication between pollen (carrying male gametes) and the pistil (female organ of flower). To prevent self-fertilization and promote outbreeding in the wild, self-incompatibility (SI) exists in many plants. SI allows the pistil of a plant to reject only pollen originating from the same plant or pollen from plant that carries the same SI genotype. The most widespread form of SI operates through a pistil-expressed S-RNase mechanism. Following pollination and pollen germination, S-RNases are translocated to the growing pollen tube, where the activity of incompatible S-RNases eventually leads to pollen tube death. Fertilization is critical for plant breeding and food production. Self-incompatibility leads to the need for artificial pollination in pear production, which is both labor- and cost-intensive.

Question: Besides degrading RNA, are there other targets for S-RNase in the pollen tube? How does the pollen tube against the cytotoxicity of S-RNase?

Findings: We found that the actin cytoskeleton is a target of S-RNase in pear and uncovered a mechanism that protects the pollen tube from S-RNase cytotoxicity involving phosphatidic acid. Pear S-RNase interacts directly with the actin protein, causing the actin cytoskeleton to depolymerize and promoting programmed cell death in the self-incompatible pollen tube. S-RNase also increases phosphatidic acid levels in the incompatible pear pollen tube, which initially play a protective role, until sustained S-RNase activity reaches the point of no return and pollen tube death.

Next steps: We have observed that the actin cytoskeleton is a target of S-RNase in pear; thus, we are investigating the possibility of overcoming self-incompatibility by stabilizing the actin cytoskeleton in pear production.

the actin cytoskeleton in pollen tubes becomes severely affected by depolymerization and gradually forms punctate actin foci throughout the entire tube during S-RNase-induced SI (Liu et al., 2007). In incompatible pollen tubes, this S-RNase activity eventually triggers structural changes in the mitochondria and the degradation of nuclear DNA (Wang et al., 2009). Actin cytoskeleton depolymerization, mitochondrial alteration, and nuclear DNA degradation are all diagnostic features of programmed cell death (PCD) in plant cells. Eukaryotic cells possess mechanisms that counteract signaling events associated with PCD, including those triggered by cytotoxins, as a survival strategy (Jones and Dangl, 2006). However, whether this type of protective mechanism counteracts the SI response in pollen remains unclear.

Phospholipase D (PLD) is a member of a heterogeneous family of enzymes found in a wide range of organisms. The 12 PLDs in *Arabidopsis thaliana* are divided into six groups: PLDα, β, γ, δ, ε, and ζ (Qin and Wang, 2002). Some PLDs participate in basic phospholipid metabolism, whereas others play important roles in many physiological and developmental processes (Zhang et al., 2003; Li et al., 2004). PLD signal transduction pathways are largely mediated by their principle product, phosphatidic acid (PA) (Wang, 2002), an important second messenger in all eukaryotes. The importance of PA during pollen tube tip growth has been established (Monteiro et al., 2005; Helling et al., 2006; Kumar and McClure, 2010). Overall, increased PA levels elevate actin filament density, whereas reduced PA production disrupts the actin cytoskeleton structure (Li et al., 2012; Pleskot et al., 2012).

Here, we demonstrate that S-RNases directly interact with actin, and we also show that these proteins exhibit actin cytoskeleton depolymerization activity in pear pollen. Interestingly, an SI-induced increase in pollen PLDδ-derived PA levels appears to postpone actin cytoskeleton depolymerization and to delay cell death signaling in self-incompatible pollen tubes, suggesting that PA levels in pear pollen may play an intermediate, decisive role between the early stages of S-RNase-triggered SI signaling and eventual pollen tube death. Based on these results, we propose that PA initially plays a protective function in pear pollen after challenge by an incompatible S-RNase. These findings add an extra dimension to our understanding of the signaling that occurs during S-RNase-based SI in pollen.

RESULTS

PbrS-RNase Directly Depolymerizes the Actin Cytoskeleton

The actin cytoskeleton of pollen tubes forms a dynamic cell framework that supports numerous fundamental cellular processes and is essential for their highly specialized polarized tip growth. We observed massive actin depolymerization in pear pollen tubes within minutes of an incompatible PbrS-RNase challenge (Supplemental Figures 1A and 1B). Thus, we initiated this study by examining how PbrS-RNase depolymerizes the actin cytoskeleton in pear pollen tubes. We used $PbrS_7$-RNase from pear in a yeast two-hybrid (Y2H) screen to identify potential pollen-interacting partners using a pear pollen cDNA library as the prey. One of the pollen interactors isolated at high frequency (5/72) was actin (Pbr032870.1; named PbrActin1). Interaction between $PbrS_7$-RNase and PbrActin1 was further confirmed by a second round of Y2H assays, a colony-lift filter assay, and a β-galactosidase activity assay (Supplemental Figure 1C). Importantly, both $PbrS_7$-RNase and $PbrS_{34}$-RNase were found to interact directly with PbrActin1 (Supplemental Figure 1C), suggesting that the interaction between PbrS-RNase and PbrActin1 is not *S*-gene specific.

We investigated the domain of PbrS-RNase that is required or responsible for the interaction with PbrActin1. PbrS-RNase

contains one hypervariable region called the Rosaceae hypervariable region and five conserved regions: conserved region 1 (C1), conserved region 2 (C2), conserved region 3 (C3), Rosaceae conserved region 4 (RC4), and conserved region 5 (C5). Only truncated $PbrS_7$-RNase lacking the RC4 domain did not interact with PbrActin1, suggesting that RC4 is the region responsible for interaction with PbrActin1 (Figure 1A). ACTIBIND and RNASET2 are members of the RNase T2 family in fungi and humans, respectively; they are structurally similar to PbrS-RNase and possess actin binding capacity (Roiz et al., 2006; Gundampati et al., 2012; Nesiel-Nuttman et al., 2014). Structural prediction revealed analogous protein domain structures in $PbrS_7$-RNase, $PbrS_{34}$-RNase, ACTIBIND, and RNASET2 (Supplemental Figure 2). Moreover, based on protein sequence alignment and crystal structure superimposition analysis, the RC4 actin binding domain of $PbrS_7$-RNase is highly conserved in ACTIBIND and RNASET2 in terms of both sequence and structure (Figures 1B and 1C). Three conserved amino acids, L149, I154, and P156, are present in the RC4 domains of these RNase T2 proteins (Figure 1B). Although mutation of L149A or I154A did not affect the ability of $PbrS_7$-RNase to bind to PbrActin1, when the proline at position 156 was substituted with an alanine (P156A), the interaction between $PbrS_7$-RNase and PbrActin1 was severely disturbed (Figure 1A). These results suggest that P156 of PbrS-RNase is essential for its proper physical interaction with PbrActin1.

We next investigated whether PbrS-RNase directly depolymerizes actin filaments. Depolymerization of actin filaments was observed with PbrS-RNase that had been extracted and purified from pear pistils, a reaction that was concentration dependent (Figure 2A). Furthermore, F-actin displayed continuous fragmentation in the presence of pistil PbrS-RNase with time (Figures 2B and 2C). We then assessed whether PbrS-RNase possesses F-actin-severing activity using total internal reflection fluorescence (TIRF) microscopy. In the absence of PbrS-RNase, actin-severing activity was extremely low, whereas there was a significant increase in severing frequency along actin filaments in the presence of PbrS-RNase (Figures 2D and 2E). These results confirm that PbrS-RNase possesses intrinsic F-actin-depolymerizing activity.

To confirm that the observed F-actin-severing activity was solely due to PbrS-RNase, we expressed PbrS-RNase in *Escherichia coli* and purified the recombinant protein (Figure 3A). First, we confirmed that recombinant PbrS-RNase exhibits RNase activity (Figure 3B). The recombinant $PbrS_7$-RNase strongly bound to actin with an equilibrium dissociation constant (K_d) of 2.2 ± 0.7 μM (Figure 3C). Addition of recombinant PbrS-RNase to in vitro pollen tube cultures resulted in similar SI responses, i.e., pollen tube growth inhibition (Supplemental Figures 3A and 3B) and actin depolymerization (Figures 3D and 3E).

PCD is a highly conserved process used to kill unwanted cells in a precisely regulated manner, and we previously demonstrated that PCD plays a key role in S-RNase-based SI in pear (Wang et al., 2009). Thus, we also evaluated whether recombinant PbrS-RNase induces PCD in pear pollen tubes. We evaluated the induction of DNA strand breaks during PCD using the terminal-deoxynucleotidyl transferase-mediated nick-end labeling (TUNEL) staining technique (Supplemental Figure 3C). Recombinant PbrS-RNase induced pollen tube death during SI (Supplemental Figure 3D); by contrast, no inhibitory effects on pollen tubes were observed using the empty vector expression product (His) or compatible (SC) treatment (Figures 3D and 3E; Supplemental Figure 3). These results demonstrate that recombinant PbrS-RNase with cytotoxic activity can be heterologously produced in *E. coli*.

Actin Binding Properties of Recombinant PbrS-RNase

We further analyzed the actin binding properties of wild-type and mutant (with mutations in the three predicted actin binding domain residues, L149A, I154A, and P156A) forms of recombinant $PbrS_7$-RNase (Figure 4A) and $PbrS_{34}$-RNase (Supplemental Figure 4A). We also combined dynamic actin depolymerization assays (Figure 4C), microscopy (Figures 4D and 4E), and TIRF microscopy analysis (Supplemental Figures 5A and 5B) to demonstrate that the actin binding domain RC4, containing P156, is crucially important for PbrS-RNase binding and F-actin-depolymerization activity. The actin-depolymerization activity of samples harboring L149A and I154A was indistinguishable from that of wild-type PbrS-RNase. These results suggest that this F-actin-severing activity is due to binding by PbrS-RNase and that P156 of PbrS-RNase is essential for actin depolymerization.

PbrS-RNase-Induced Depolymerization of the Actin Cytoskeleton Is Independent of RNase Activity

The RNase activity of petunia (*Petunia hybrida*) S_3-RNase is essential for SI; replacement of the conserved histidine in the C3 region with an asparagine abolishes its RNase activity, resulting in failure to reject S_3 pollen (Huang et al., 1994; McCubbin et al., 1997). Based on protein sequence alignment, $PbrS_7$-RNase and $PbrS_{34}$-RNase share the conserved His116 in the C3 region of petunia S_3-RNase (Supplemental Figure 6). Thus, to determine whether the RNase activity of PbrS-RNase is important for its actin-severing activity, His-116 was mutated to Arg in $PbrS_7$-RNase (Figure 4A) and $PbrS_{34}$-RNase (Supplemental Figure 4A), and these mutant forms were then heterologously expressed in *E. coli* and purified. This mutation substantially reduced RNase activity, whereas mutations in the actin binding domain had a negligible effect on RNase activity (Figure 4B; Supplemental Figure 4B). Using a dynamic actin depolymerization assay (Figure 4C), visual detection via microscopy (Figures 4D and 4E), and TIRF microscopy analysis (Supplemental Figure 5), we observed normal actin depolymerization and F-actin-severing activity in PbrS-RNase with the H116R mutation. These findings suggest that the RNase activity of PbrS-RNase is not essential for its actin-depolymerization activity.

To verify this hypothesis, we investigated the effect of the H116R mutation on actin depolymerization activity during SI. PbrS-RNase lacking RNase activity was still able to elicit cytoskeletal changes similar to those of the fully functional PbrS-RNase during SI (Figure 4F). Moreover, PbrS-RNase with the P156A mutation mitigated incompatible pollen PCD compared with the wild type and other mutant PbrS-RNase (Figure 4G). This evidence supports the conclusions that the RNase activity and actin depolymerization activity of PbrS-RNase do not affect each other and that the actin depolymerization activity of PbrS-RNase plays an important role in promoting PCD in the SI of pear pollen tubes.

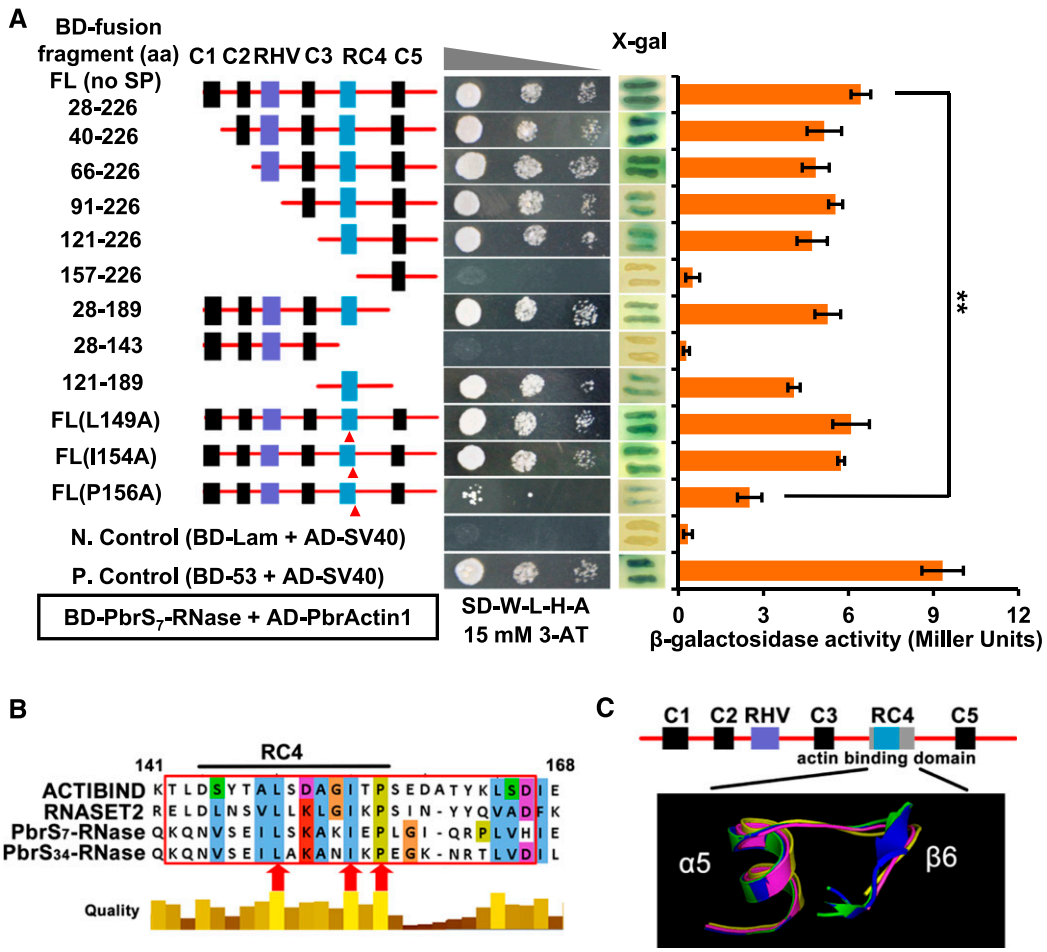

Figure 1. The RC4 Domain of PbrS-RNase Is Critical for Interaction with PbrActin1.

(A) Dissection of the functional domains of $PbrS_7$-RNase required for interaction with PbrActin1 in Y2H assays. The wedge indicates the gradient dilution at 1, 0.1, and 0.01. A positive interaction between PbrS-RNase and actin was confirmed by a filter assay. The interaction strength was quantified based on β-galactosidase activity. The experiments were repeated four times, with similar results. Asterisks indicate significant statistical difference between wild-type $PbrS_7$-RNase and P156A mutation as evaluated by ANOVA and Tukey's test: **$P < 0.01$; error bars indicate SE.

(B) Sequence alignment of $PbrS_7$-RNase, $PbrS_{34}$-RNase, *Aspergillus niger* ACTIBIND, and human RNASET2. The black line represents the RC4 domain of PbrS-RNase. The red box represents the sequence of ACTIBIND identified as binding to actin.

(C) Superimposition of the structures of the RNase binding actin domains of $PbrS_7$-RNase (blue), $PbrS_{34}$-RNase (green), ACTIBIND (purple), and RNASET2 (yellow). The ACTIBIND protein (Protein Data Bank entry 3d3z) was used as a crystal structure model.

SI Challenge Results in PA Accumulation in the Pollen Tube

In addition to structural changes in the actin cytoskeleton, we observed a 2-fold increase in PA levels in pollen tubes within 5 min after challenge with incompatible PbrS-RNase, whereas no change in PA levels was observed in pollen tubes treated with compatible PbrS-RNase (Figures 5A and 5B). In addition, the PA levels increased in a time-dependent manner in incompatible pollen tubes after SI challenge. These results suggest that phospholipids are involved in the SI response in pear pollen.

Two distinct signaling pathways lead to PA production in plants. The first pathway involves the direct cleavage of structural phospholipids by PLD, and the second involves a cascade of reactions catalyzed by phospholipase C and diacylglycerol kinase. 1-Butanol is an alcohol isomer that results in the production of phosphatidylbutanol (PBut) instead of phosphatidic acid (PA) and thus inhibits PLD-dependent PA signaling (Munnik, 2001). To evaluate the possible contribution of PLD to SI-induced PA production, we added 0.10% (v/v) 1-butanol to pollen tube cultures. This concentration of 1-butanol had negligible effects on both pollen germination and pollen tube growth in the absence of PbrS-RNase (Supplemental Figures 7A and 7B). 2-Butanol and *t*-butanol are isomers of 1-butanol, but they did not inhibit PLD-dependent PA production (Gardiner et al., 2003); thus, they did not affect the pollen germination rate and pollen tube growth (Supplemental Figures 7A and 7B). By adding PA, the inhibition of pollen germination and pollen tube growth by 1-butanol could be rescued in a PA concentration dependent manner (Supplemental Figures 7C and 7D).

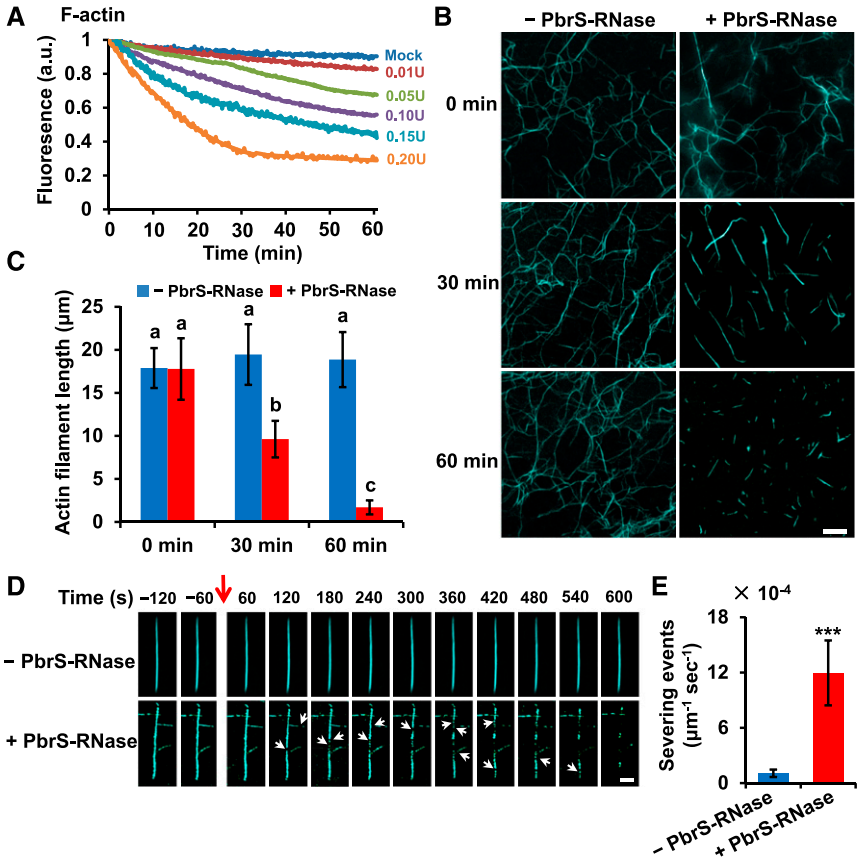

Figure 2. PbrS-RNase Directly Depolymerizes Actin Filaments.

(A) $PbrS_7$-RNase depolymerizes F-actin in a concentration-dependent manner. Depolymerization of actin was monitored based on the decrease in pyrene fluorescence. The figure shows the results from a representative experiment ($n = 5$).

(B) and **(C)** Addition of 0.15 units of $PbrS_7$-RNase results in actin filament depolymerization. Micrographs and the mean actin filament length (each experiment consisting of ≥200 determinations) are shown in **(B)** and **(C)**, respectively. Different letters indicate significant differences, as determined by ANOVA followed by Tukey's multiple comparison test ($P < 0.05$; $n = 3$; error bars indicate SE). Bar = 2 μm.

(D) 0.15 units of $PbrS_7$-RNase significantly increases severing events in actin filaments compared with the control, as determined by TIRF microscopy analysis. F-actin was assembled from 0.5 μM G-actin (FITC-phalloidin labeled) and attached to glass slides coated with myosin. At the treatment times (vertical red arrow), the reaction mixture was replaced with 0.15 units of $PbrS_7$-RNase. The white arrows indicated the depolymerization sites of the F-actin. Bar = 1 μm.

(E) Quantification of the depolymerizing efficiencies of $PbrS_7$-RNase shown in **(D)**. ***$P < 0.001$ by Student's *t* test compared between −$PbrS_7$-RNase and +$PbrS_7$-RNase. Error bars indicate SE.

However, the levels of both PA and PBut in pollen tubes increased during the SI response after the addition of PbrS-RNase (Figure 5C), with the increases following similar kinetics during the course of the SI response (Figure 5D). These results suggest that PLD activity is involved in SI-induced PA production.

SI-Induced PA Production in Pollen Is Mediated by PbrPLDδ1

We then investigated which *PLD* gene is responsible for SI-induced PA in pear pollen. Eighteen *PLD* genes have been identified in the pear genome (Wu et al., 2013) (Supplemental Figure 8A). Based on phylogenetic and domain conservation analyses of predicted PLD protein sequences (Eliás et al., 2002; Li et al., 2007), we classified these genes into three subgroups: C2-PLDs, PXPH-PLDs, and SP-PLDs (Supplemental Figures 8B and 8C). We then assigned individual gene names to pear *PLD*s using the nomenclature and numbering conventions for Arabidopsis and rice (*Oryza sativa*). Seven of the 18 *PLD* genes were highly expressed in pollen, as revealed by RT-qPCR (Figure 6A). However, only *PbrPLDδ1*, encoding an enzyme associated with the plasma membrane (Supplemental Figure 9), was expressed at significantly higher levels in response to challenge with incompatible S-RNase; by contrast, the expression of all other *PbrPLD* genes was unchanged in pear pollen exposed to compatible PbrS-RNase (Figure 6A). These results suggest that SI-induced PA production in pear pollen is likely mediated by PbrPLDδ1.

To confirm the contribution of PbrPLDδ1 to SI-induced PA production, we employed the antisense (as) oligodeoxynucleotide (ODN) method to specifically knock down the expression of *PbrPLD* genes in pear pollen, a technique that is widely used to specifically

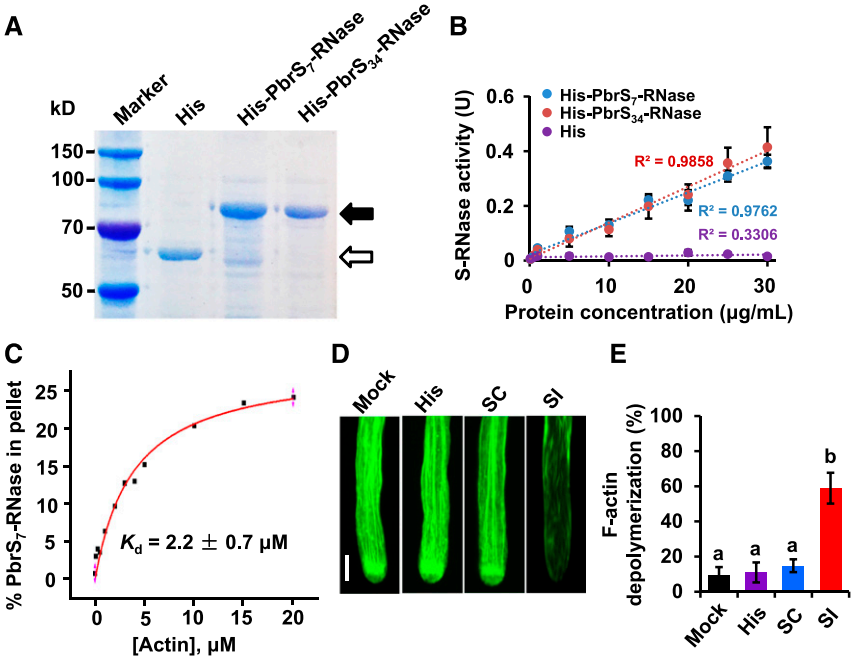

Figure 3. Recombinant PbrS-RNase Binds to F-Actin and Depolymerizes the Actin Cytoskeleton in an *S*-Specific Manner.

(A) Purified PbrS-RNases from *E. coli*. $PbrS_7$-RNase and $PbrS_{34}$-RNase were fused with the TF-His tag and expressed in *E. coli* Rosetta (DE3) cells. Proteins were separated by 10% SDS-PAGE, followed by Coomassie blue staining. The solid arrow indicates the protein band corresponding to PbrS-RNases, and the unfilled arrow indicates TF-His tag expressed by the empty vector.

(B) Recombinant PbrS-RNases retain RNase activity. Correlation analysis was used to estimate the RNase efficiency of the purified PbrS-RNases toward yeast RNA. The correlation coefficients (R^2) for $PbrS_7$-RNases (blue) and S_{34}-RNase (red) were greater than 0.97, demonstrating their efficiency; 10 μg (corresponding to 0.15 units of enzymatic activity) PbrS-RNase was used for treatment in subsequent analyses.

(C) High-speed cosedimentation assays to determine the apparent affinity of $PbrS_7$-RNase binding to F-actin. Various amounts of phalloidin-stabilized F-actin were combined with 0.5 μM (corresponding to 15 μg/mL) $PbrS_7$-RNase. The amount of bound protein in the pellet was determined by densitometry. The percentage of bound $PbrS_7$-RNase was plotted against the concentration of actin and fitted with a hyperbolic curve.

(D) Recombinant PbrS-RNases induce F-actin depolymerization in self-incompatible pollen tubes. Typical images of actin cytoskeletal configuration in pollen tubes after 30 min of various treatments are shown. Bar = 20 μm.

(E) Quantification of pollen tubes showing F-actin depolymerization in response to 30 min of various treatments. Purified PbrS-RNase causes a significant increase in F-actin depolymerization. Different letters indicate significant differences, as determined by ANOVA followed by Tukey's multiple comparison test ($P < 0.05$; $n = 4$); error bars indicate SE.

suppress target gene expression in pollen tubes (Estruch et al., 1994; Moutinho et al., 2001; de Graaf et al., 2006; Pleskot et al., 2010). After as-ODN treatment, the expression levels of target genes decreased by more than 65% compared with the control and samples treated with sense-ODNs (Supplemental Figures 10A and 10B). Moreover, the use of *PbrPLD* gene-specific ODNs only inhibited the expression of specific *PbrPLD* genes and did not affect any other *PbrPLD* genes in pollen (Supplemental Figure 10C). The specific knockdown of *PbrPLDδ1* resulted in a significant decrease in SI-induced PA and PBut production, whereas knockdown of *PbrPLDα1* or *PbrPLDβ1* had no effect on PA or PBut levels (Figures 6B to 6D). These results indicate that SI-induced PA is specifically mediated by *PbrPLDδ1* in pear pollen.

PbrPLDδ1-Derived PA Delays SI-Induced PCD in Pollen Tubes

We then assessed the potential roles of PbrPLDδ1 and PA in SI-induced PCD in pear pollen tubes. Unexpectedly, specific knockdown of *PbrPLDδ1* accelerated pollen tube death during the early stages of SI (Figures 7A and 7B). This acceleration was alleviated by the addition of 20 μM exogenous PA during SI (Figure 7B). The timing of pollen tube death and the effect of PbrPLDδ1 on timing were confirmed using fluorescein diacetate, a pollen viability marker (Supplemental Figures 11A and 11B). These results suggest that an increase in PbrPLDδ1 activity and associated PA levels delays the PCD response after incompatible PbrS-RNase challenge. To further investigate whether PLD-derived PA is involved in this reaction, we treated pollen with both incompatible PbrS-RNase and 1-butanol. The time needed to trigger PCD was significantly shorter compared with pollen treated with incompatible PbrS-RNase alone (Figure 7C), whereas the addition of exogenous PA to the incompatible PbrS-RNase/1-butanol reaction mixture partially alleviated the effect of 1-butanol (Figure 7C), with an optimal concentration of 20 μM PA (Supplemental Figure 12). The PCD ratios of pollen tubes treated with 2-butanol or *t*-butanol were similar to those of the control (Figure 7D), suggesting that PLD-derived PA plays a pivotal role in the SI response

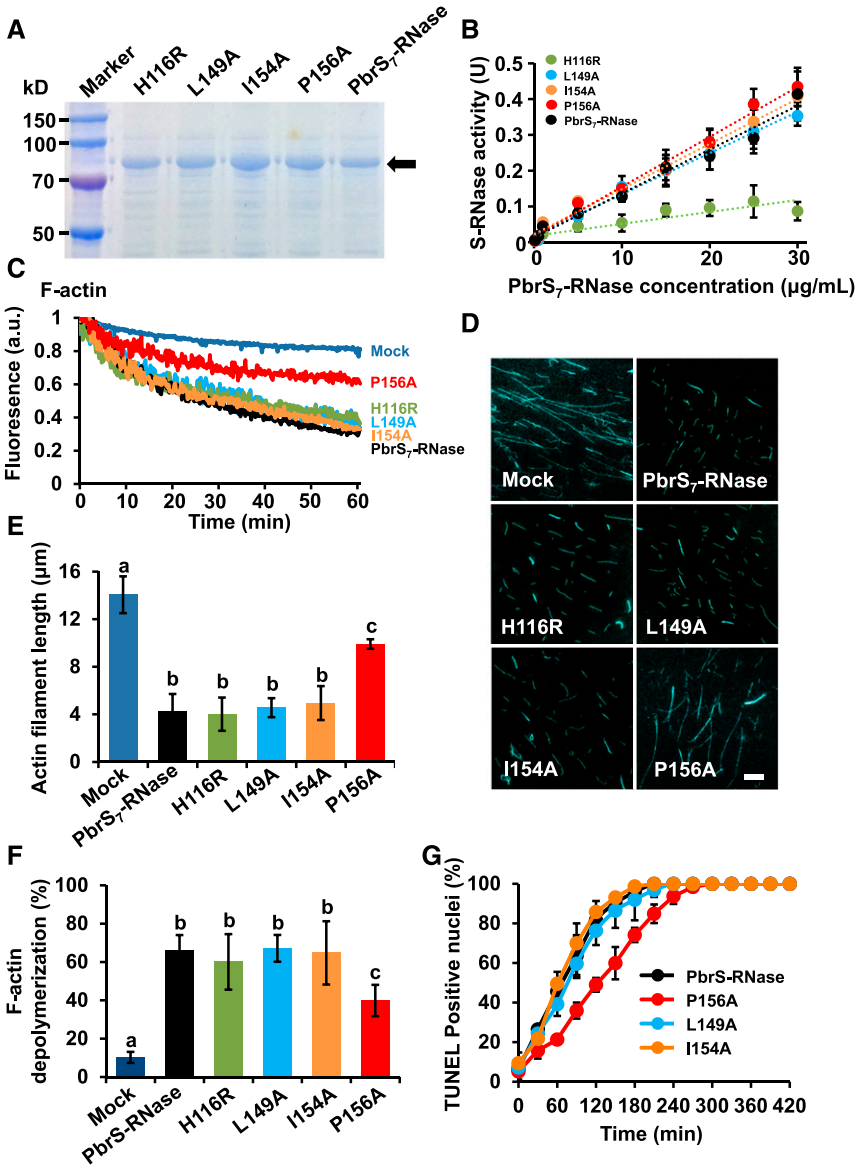

Figure 4. The P156A Mutation Abolishes the Actin-Depolymerization Activity of PbrS-RNase.

(A) Mutant $PbrS_7$-RNases were expressed in *E. coil* and purified.

(B) Mutation in the actin binding domain of $PbrS_7$-RNase has a negligible effect on RNase activity, whereas a mutation (H116R) in the catalytic site abolishes the RNase activity of $PbrS_7$-RNases (n = 3).

(C) The F-actin depolymerization activity of mutated $PbrS_7$-RNase monitored based on a decrease in pyrene fluorescence. $PbrS_7$-RNase P156A lacks actin depolymerization activity. The figure shows the results from a representative experiment (n = 5).

(D) and **(E)** Mutant $PbrS_7$-RNase depolymerizes F-actin based on microscopy detection. Addition of the same concentration of mutated $PbrS_7$-RNase for 60 min indicated that the P156A mutation abolishes actin filament depolymerization activity. Micrographs and the mean actin filament length (each experiment consisting of ≥200 determinations) are shown in **(D)** and **(E)**, respectively. Different letters in **(E)** indicate significant differences, as determined by ANOVA followed by Tukey's multiple comparison test ($P < 0.05$; n = 3); error bars indicate SE. Bar = 2 μm.

(F) Treatment with the P156A mutant form of PbrS-RNase leads to a significant decrease in actin filament depolymerization in incompatible pollen after 30 min of treatment. Different letters indicate significant differences, as determined by ANOVA followed by Tukey's multiple comparison test ($P < 0.05$; n = 4); error bars indicate SE.

(G) Time-course analysis showing that the P156A mutant form of PbrS-RNase mitigates incompatible pollen PCD (in median lethal time [LT_{50}] analysis; $P < 0.01$ for the P156A mutant form of PbrS-RNase compared with wild-type PbrS-RNase, by Student's t test; n = 4; error bars indicate SE). Experiment was repeated four times; each experiment included at least 100 measurements.

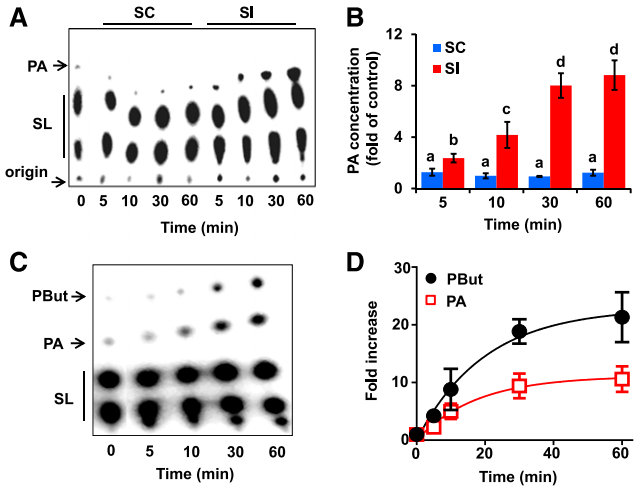

Figure 5. Self-Incompatible Pollen Tubes Exhibit Increased PA Accumulation.

(A) Incompatible PbrS-RNase increases PA levels in pear pollen. Lane 1, control in the absence of PbrS-RNase. Lanes 2 to 5 show the results after 5, 10, 30, and 60 min of treatment with 0.15 units of compatible PbrS-RNase. Lanes 6 to 9 show the results after 5, 10, 30, and 60 min of treatment with 0.15 units of incompatible PbrS-RNase. SC, compatible PbrS-RNase treatment; SI, incompatible PbrS-RNase treatment.

(B) Quantification statistics of the PA levels from **(A)**. PA levels are expressed as fold increases compared with control samples. PA levels significantly increased after 5 min of SI treatment. Different letters indicate significant differences, as determined by ANOVA followed by Tukey's multiple comparison test ($P < 0.05$; $n = 3$); error bars indicate SE.

(C) Thin-layer chromatography images of time-dependent increases in PA and PBut levels after incompatible PbrS-RNase treatment. SL, structural phospholipids.

(D) Quantification statistics for the time course of increases in PBut and PA levels. PA and PBut levels are expressed as fold increases compared with control samples. Both PA and PBut levels in pollen tubes increased with similar kinetics under incompatible PbrS-RNase treatment. All data are the means of three independent experiments. Error bars indicate SE.

in pear. However, knockdown of *PbrPLDα1* or *PbrPLDβ1* expression did not affect the timing of pollen tube PCD during an SI challenge (Figure 7D). These results indicate that *PbrPLDδ1* expression is specifically induced in pollen tubes upon SI challenge, and they suggest that PbrPLDδ1 plays a role in the timing of signaling events mediated by PA upon SI challenge.

To examine whether other acidic lipids are involved in regulating SI, we treated samples with inositol-1,4,5-trisphosphate (IP_3), phosphatidylinositol-3-phosphate (PI_3P), phosphatidylinositol-4-phosphate (PI_4P), phosphatidylinositol-5-phosphate (PI_5P), phosphatidylinositol-3,4-phosphate [$PI_{(3,4)}P_2$], phosphatidylinositol-3,5-phosphate [$PI_{(3,5)}P_2$], phosphatidylinositol-4,5-phosphate [$PI_{(4,5)}P_2$], phosphatidylinositol-3,4,5-trisphosphate [$PI_{(3,4,5)}P_3$], sphingosine-1-phosphate (S1P), and PA and examined their effects on growth (Figure 7E) and PCD (Figure 7F) in incompatible pollen tubes. PA significantly rescued SI-induced growth arrest and mitigated SI-induced PCD, whereas the other acidic lipids had negligible effects on SI signaling. These findings indicate that PA is an acidic lipid that specifically provides pollen tubes with a basic level of protection against PbrS-RNase-triggered PCD.

PbrPLDδ1-Derived PA Reduces SI-Induced PCD by Stabilizing the Actin Cytoskeleton

Depolymerization of the actin cytoskeleton during the early stages of the SI response is thought to play a decisive role in PCD induction in pollen (Thomas et al., 2006; Wang et al., 2010). Furthermore, PA might help stabilize the actin cytoskeleton (Pleskot et al., 2012, 2013). Our results suggest that an increase in PbrPLDδ1-derived PA levels extends the lifespan of self-incompatible pollen tubes. We therefore hypothesized that PA might affect actin cytoskeleton dynamics during the early stages of the SI response. Disruption of actin cytoskeleton dynamics in control self-incompatible pollen tubes (i.e., 50% of actin showing depolymerization) was observed after 25.2 ± 1.9 min after SI challenge. However, in *PbrPLDδ1*-knockdown pollen tubes, 50% of the actin cytoskeleton had depolymerized at 14.1 ± 1.1 min after the SI challenge (Figures 8A and 8B). This acceleration of actin depolymerization was reversed in *PbrPLDδ1*-knockdown pollen tubes by the addition of exogenous PA (Figures 8A and 8B). Similar results were obtained by measuring changes in fluorescence intensity in actin filaments (Figure 8C). 1-Butanol treatment also significantly accelerated depolymerization of the actin cytoskeleton, but 2-butanol or *t*-butanol did not change the speed of actin depolymerization during SI response (Supplemental Figure 13). The time required for 50% actin depolymerization did not change in *PbrPLDα1*- or *PbrPLDβ1*-knockdown pollen tubes after SI challenge (Supplemental Figure 13). However, coincubation with PA did not directly inhibit actin filament depolymerization by PbrS-RNase (Figure 8D), suggesting that stabilization of the actin cytoskeleton by PA during the early stages of SI challenge is mediated by additional PA target factors in the pollen tube.

DISCUSSION

The key role of S-RNase in determining the rejection of self-incompatible pollen has been known for more than two decades, and the role of S-RNases in degrading rRNA in self-incompatible pollen tubes is also well established. The results of this study provide evidence that PbrS-RNases play additional roles in severing actin filaments during the SI response. We demonstrated that PbrS-RNase directly interacts with PbrActin1, causing the actin cytoskeleton to depolymerize and inducing PCD in self-incompatible pear pollen tubes. In addition, we showed that the actin-depolymerization activity of PbrS-RNase is not associated with its RNase activity. During the early stages of PbrS-RNase signaling, we observed a specific increase in PbrPLDδ1 expression and activity in self-incompatible pollen tubes, which resulted in an increase in PA levels. In turn, PbrPLDδ1 postponed actin cytoskeleton depolymerization via PA, thus delaying self-incompatible pollen tube death. Thus, PbrActin1 is a direct target of PbrS-RNase in the pear pollen tube. We propose that PLDδ activity and an increase in PA levels initially protect pollen tubes from PbrS-RNase signaling during the early stage of the SI response until PbrS-RNase levels and activity rise to the point of no return.

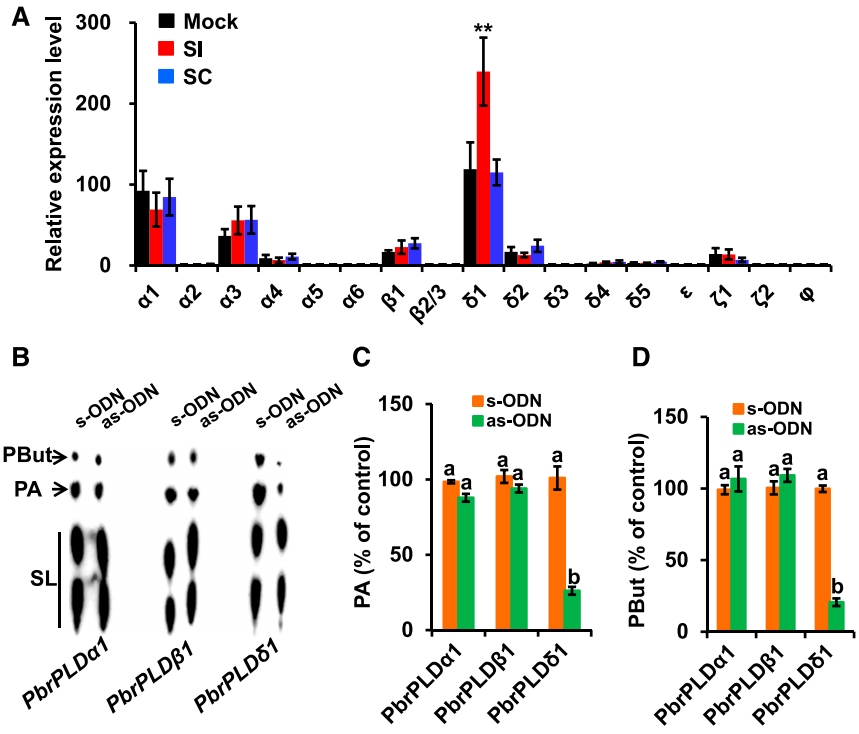

Figure 6. The SI-Induced Increase in PA Levels Is Mediated by PbrPLDδ1 in Pollen.

(A) RT-qPCR analysis of *PbrPLD* expression in control and treated (compatible and incompatible, 30 min) pollen samples at 4 h post-culture. *PbrPLDδ1* mRNA levels significantly increased in response to SI treatment. Asterisks indicate significant statistical difference between SI treatment and mock as evaluated by ANOVA and Tukey's test: $^{**}P < 0.01$; $n = 4$; error bars indicate SE.

(B) Images of PBut and PA signals for the three genotypes after 60 min of incompatible PbrS-RNase treatment. Pear pollen was cultured for 4 h with 0.10% (v/v) 1-butanol plus 50 μM antisense (as) or sense (s) ODNs targeting *PbrPLDα1*, *PbrPLDβ1*, or *PbrPLDδ1* before treatment.

(C) and **(D)** PA and PBut levels are expressed as percentages compared with control samples. The as-ODN-mediated knockdown of *PbrPLDδ1* significantly decreased PA levels in samples showing an SI response at 60 min. Different letters indicate significant differences, as determined by ANOVA followed by Tukey's multiple comparison test ($P < 0.05$; $n = 3$); error bars indicate SE.

PbrS-RNase Directly Interacts with Actin PbrActin1 and Depolymerizes the Actin Cytoskeleton in the Pollen Tube

PbrS-RNases belong to the T2 family of RNases. Several members of this family have roles in addition to RNA degradation. For example, ACTIBIND and RNASET2 directly bind to actin to disrupt the actin cytoskeleton (Roiz et al., 2006; Gundampati et al., 2012; Nesiel-Nuttman et al., 2014). However, an intact actin cytoskeleton is required for multiple cellular functions (Li et al., 2015; Yanagisawa et al., 2015), and subtle modifications in actin cytoskeleton dynamics can determine cell survival or death (Thomas et al., 2006; Franklin-Tong and Gourlay, 2008). The SI response in pollen tubes is characterized by depolymerization of the actin cytoskeleton. For example, in the SI mechanism of poppy (*Papaver rhoeas*), PrsS, an *S*-protein in the pistil, acts as an extracellular ligand, triggering a rapid but transient increase in cytoplasmic free calcium levels, leading to the induction of actin depolymerization and ultimately PCD (Thomas et al., 2006). Previous studies in our laboratory (Liu et al., 2007; Wang et al., 2010) and our results (Supplemental Figures 1A and 1B) demonstrate that the dynamics of the actin cytoskeleton in pear pollen tubes is disturbed by the action of incompatible PbrS-RNase.

Like ACTIBIND and RNASET2, PbrS-RNase directly interacts with actin (Supplemental Figure 1C), and the amino acid crucial for interaction with PbrActin1 is P156 (Figure 1A). The conservation of P156 among PbrS-RNase, ACTIBIND, and RNASET2 (Figure 1B) suggests that it is also likely a key site through which ACTIBIND and RNASET2 interact with actin. PbrS-RNase was found to interact directly with actin in the pollen of two other Rosaceae species, sweet cherry (*Prunus avium*; Matsumoto and Tao, 2012) and apple (*Malus domestica*; Meng et al., 2014). However, observations in *Solanum chacoense* suggest that the interaction between S-RNase and actin is mediated by the actin binding protein eEF1A (Soulard et al., 2014). It should be noted that P156 is located in the RC4 region of PbrS-RNase (Figure 1C); this region is, to some extent, unique to S-RNases in Rosaceae, suggesting that the RC4 domain and its importance in actin binding and depolymerization activity are different from those of S-RNase-based SI mechanisms found in other flowering plant species. Furthermore, our coincubation assay showed that both pistil-derived (Figure 2) and *E. coli*-expressed PbrS-RNase (Figure 3D; Supplemental Figure 5) can degrade the actin cytoskeleton. Nonetheless, the actin depolymerization activity of PbrS-RNase is not necessary and does not affect its RNase activity (Figure 4), suggesting the existence of diverse targets of

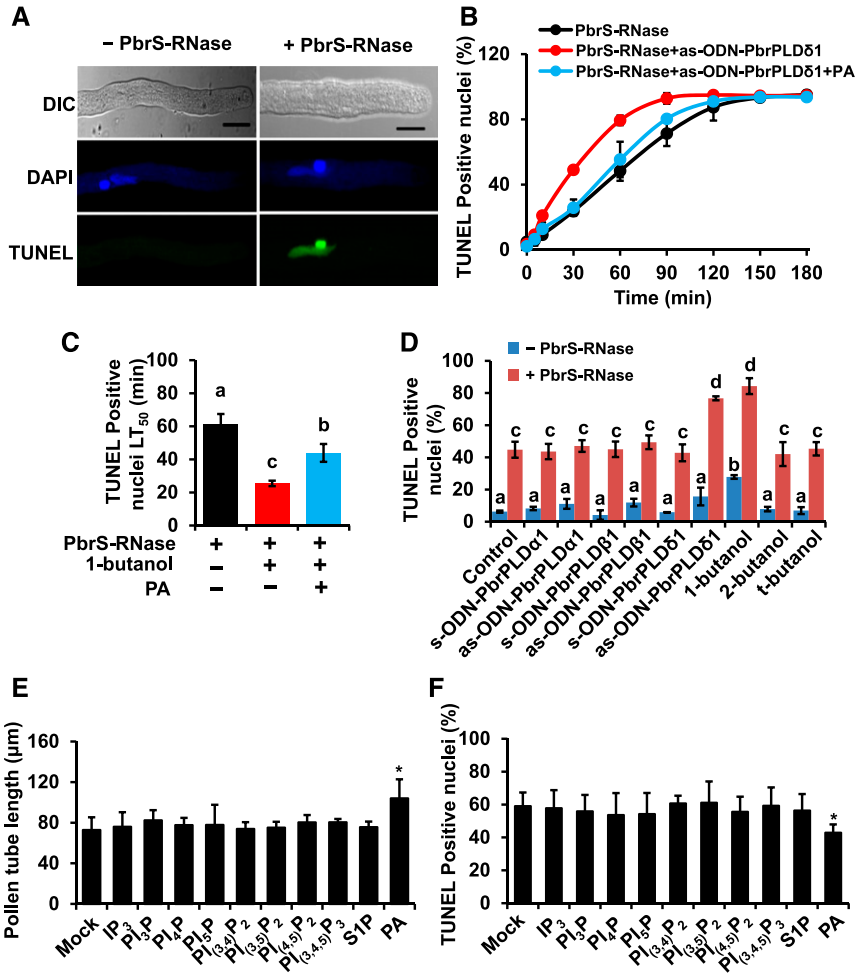

Figure 7. PbrPLDδ1-Derived PA Reduces SI-Induced PCD in Pollen Tubes.

(A) DNA fragmentation detected by TUNEL labeling. Images of negative (left) and positive (right) TUNEL signals. DAPI (4′,6-diamidino-2-phenylindole) staining showing that TUNEL-positive signals correspond to nuclear DNA. Bar = 20 μm.

(B) Time-course analysis showing that antisense-mediated knockdown of *PbrPLDδ1* increases the sensitivity of pear pollen tubes to PbrS-RNase-induced PCD (LT_{50} decreased from 62.3 ± 7.7 min in the wild-type control to 29.8 ± 5.9 min in the *PbrPLDδ1*-knockdown group; $P < 0.001$, by Student's *t* test; $n = 3$; error bars indicate SE). This effect was mitigated by the addition of 20 μM PA (LT_{50} is 53.2 ± 5.7 min; there is no significant difference compared with wild-type control, by Student's *t* test; $n = 3$; error bars indicate SE).

(C) LT_{50} analysis revealing that the 1-butanol-mediated inhibition of PLD activity significantly reduces LT_{50} times of pollen tube PCD, but this acceleration was alleviated by the addition of 20 μM exogenous PA during SI. Different letters indicate significant differences, as determined by ANOVA followed by Tukey's multiple comparison test ($P < 0.05$; $n = 3$); error bars indicate SE.

(D) Quantification of PCD in pollen tubes after 60 min of various treatments. Knockdown of *PbrPLDδ1* and the addition of 0.25% 1-butanol led to a significant increase in cell death. The experiment was repeated three times; each experiment included at least 100 measurements. Different letters indicate significant differences, as determined by ANOVA followed by Tukey's multiple comparison test ($P < 0.05$; $n = 3$); error bars indicate SE.

(E) Only PA significantly mitigates the inhibition of self-incompatible pollen tube growth. The culture solution included 0.15 units of incompatible PbrS-RNase and one of the following lipids: 50 μM IP_3, 10 μM PI_3P, 10 μM PI_4P, 10 μM PI_5P, 50 μM $PI_{(3,4)}P_2$, 50 μM $PI_{(3,5)}P_2$, 50 μM $PI_{(4,5)}P_2$, 50 μM $PI_{(3,4,5)}P_3$, 1 μM S1P, or 20 μM PA. The pollen tubes were cultured for 3 h. PA significantly mitigated the inhibition of self-incompatible pollen tube growth, but other acidic lipids did not. Asterisk indicates significant statistical difference between PA treatment and mock as evaluated by ANOVA and Tukey's test: *$P < 0.05$; $n = 3$; error bars indicate SE.

(F) PA significantly reduces PCD signaling in self-incompatible pollen tubes. Pollen tubes at 3 h post-culture were incubated with different acidic lipids for 10 min, followed by the addition of incompatible PbrS-RNase at 0.15 units and culture for 1 h. The samples were processed for TUNEL staining, followed by statistical analysis. PA significantly decreased the positive TUNEL ratio for self-incompatible pollen tubes, but other acidic lipids did not. Experiment was repeated three times; each experiment included at least 100 measurements. Asterisk indicates significant statistical difference between PA treatment and mock as evaluated by ANOVA and Tukey's test: *$P < 0.05$; $n = 3$; error bars indicate SE.

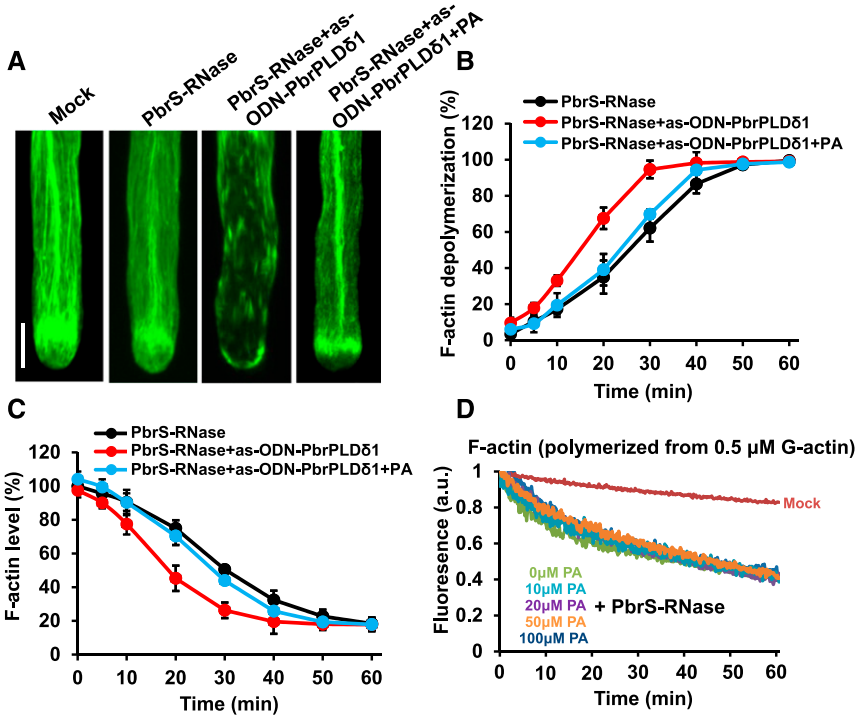

Figure 8. Effects of PbrPLDδ1-PA on the Actin Cytoskeleton during SI.

(A) Typical images (after 10 min of treatment) of actin cytoskeletal configurations in a normal cultured pollen tube, incompatible PbrS-RNase-challenged pollen tube, *PbrPLDδ*-as-ODN-mediated knockdown pollen tube under incompatible PbrS-RNase challenge, and *PbrPLDδ1*-as-ODN-mediated knockdown pollen tube under incompatible PbrS-RNase plus 20 μM PA treatment. Bar = 20 μm.

(B) and **(C)** Time-course analysis showing that as-ODN-mediated knockdown of *PbrPLDδ1* accelerates PbrS-RNase-induced F-actin depolymerization **(B)** and reduces F-actin levels **(C)** during SI. This effect was mitigated by the addition of 20 μM PA. Experiment was repeated five times; each experiment included at least 100 measurements for F-actin depolymerization analysis. Knockdown of *PbrPLDδ1* led to a significantly accelerated median F-actin depolymerization time (LT_{50}) and F-actin level compared with wild-type control ($P < 0.001$ for F-actin depolymerization time, $P < 0.001$ for F-actin level, by Student's *t* test; $n = 5$; error bars indicate SE).

(D) Various concentrations of PA do not directly inhibit PbrS-RNase-mediated depolymerization of F-actin. PbrS-RNase (0.15 units) was incubated with PA at various concentrations for 10 min, followed by coincubation with F-actin (pyrene-labeled) for 5 min before 50-fold dilution in 1× KMEI buffer. The results from a representative experiment ($n = 5$) are shown.

PbrS-RNase during the SI. These results suggest that two separate mechanisms in pear pollen likely induce PCD during SI response, i.e., RNA degradation and actin disassembly.

Interaction of PbrS-RNase with PbrActin1 Does Not Rely on *S*-Haplotype Recognition

The interaction of PbrS-RNase with PbrActin1 is not *S*-specific (Supplemental Figure 1C), suggesting that this interaction does not rely on *S*-haplotype recognition. Upon pollen tube growth in the pistil, S-RNases enter both compatible and incompatible tubes (Gray et al., 1991; Luu et al., 2000; Goldraij et al., 2006; Boivin et al., 2014). In compatible pollen tubes, S-RNases are degraded by the *S*-locus F-box protein (Qiao et al., 2004; Sijacic et al., 2004), or they remain compartmentalized in the pollen vacuole (Goldraij et al., 2006), suggesting that the level of actin depolymerization is low. Conversely, in incompatible pollen tubes, S-RNases remain in the cytoplasm or are released from vacuoles into the cytoplasm, inducing high levels of actin depolymerization. Thus, we suggest that the degree of depolymerization of the actin cytoskeleton depends on the level of PbrS-RNase in the cytoplasm of the pollen tube. In *P. rhoeas*, an ~50% reduction in F-actin levels by treatment with Latrunculin B, a chemical agent with specific actin cytoskeleton depolymerization activity, resulted in a high incidence of DNA fragmentation, even though F-actin levels returned to normal after the removal of Latrunculin B. This finding indicates that ~50% of actin depolymerization represents an irreversible, "decision-making" step, pushing the pollen tube toward PCD (Thomas et al., 2006). In plant-pathogen systems, a zigzag model has been used to describe how the plant counteracts pathogen attack up to a point of no return. When a certain threshold is surpassed, the plant will be induced to undergo hypersensitive cell death (Jones and Dangl, 2006). Parallels exist between the SI in Rosaceae and nonhost immunity, as a fundamental feature of both processes is the ability to distinguish "self" from "non-self," and both ultimately result in the triggering of PCD to eliminate undesirable pollen or cells (Sanabria et al., 2008).

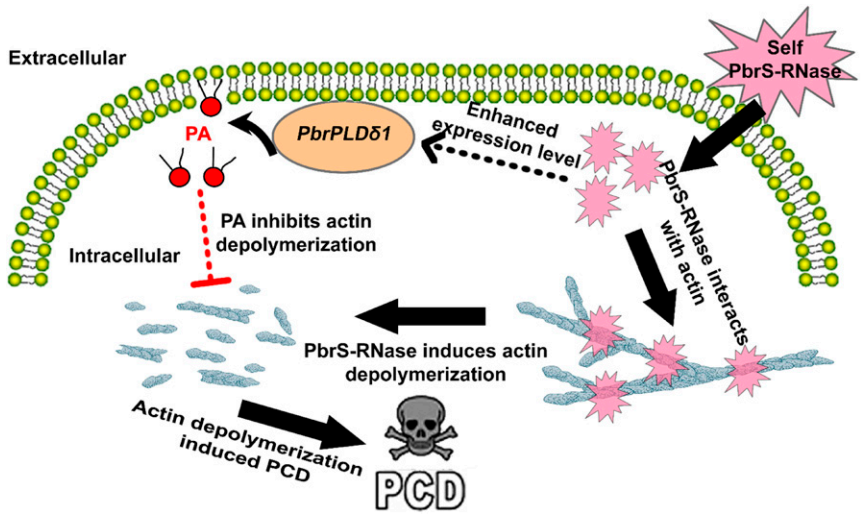

Figure 9. Schematic Diagram of the Mechanism by Which PbrPLDδ1-Derived PA Mediates Early SI Signaling in Pollen by Stabilizing the Actin Cytoskeleton.

PbrS-RNase directly interacts with actin protein, leading to actin cytoskeleton depolymerization in self-incompatible pollen tubes. However, PbrS-RNase enhances the expression of *PbrPLDδ1*, encoding a plasma membrane-localized protein, leading to an increase in PA levels. This PA prevents depolymerization of the actin cytoskeleton, thus delaying SI-induced PCD.

During SI in pear, the cessation of pollen tube growth generally occurs approximately halfway into the pistil. Thus, PbrS-RNase accumulates to a level at which depolymerization of the actin cytoskeleton is sufficient to induce PCD signaling in an incompatible pollen tube. However, in the early stage of SI in pear, i.e., when the pollen tube has not yet reached half the length of the pistil, PbrS-RNase levels in incompatible pollen tubes are low, and the PbrS-RNase-induced degree of actin depolymerization is not sufficient to induce PCD signaling and can be rescued by PbrS-RNase-elicited PA (see below). This process would delay the SI signaling pathway, leading to pollen tube death in incompatible pollen tubes when PbrS-RNase accumulates to sufficient levels.

PbrPLDδ1-Derived PA Mitigates PbrS-RNase Cytotoxicity by Stabilizing the Actin Cytoskeleton

Plants have evolved complex protective mechanisms against invasion. We have produced several lines of evidence suggesting that PbrPLDδ1-derived PA initially mediates a defense response against PCD signaling in the pollen tube promoted by PbrS-RNase. First, 1-butanol, an inhibitor of PLD-dependent PA production, accelerates PCD signaling in self-incompatible pollen tubes (Figure 7C). Second, PbrPLDδ1 is the sole pollen-expressed PLD shown to be directly involved in the PbrS-RNase-specific signaling pathway in pear, despite the expression of six other *PbrPLD* genes in pear pollen tubes (Figure 6). Specific inhibition of PbrPLDδ1 expression via as-ODN silencing impaired SI-induced PA production and accelerated PCD in self-incompatible pollen tubes (Figures 6 and 7). Moreover, complementation assays in which PA was added to pollen cultures alleviated the accelerated death of *PbrPLDδ1*-as-ODN pollen tubes during the SI response (Figure 7B). These results are important for determining the mechanism of PLD action, as other products are generated in addition to PA. However, as we did not observe a direct interaction between PbrS-RNase and PbrPLDδ1 (Supplemental Figure 14), the association between incompatible PbrS-RNase and PbrPLDδ1 in pollen remains to be elucidated.

The cytoskeleton is one of the most important targets of PLD/PA (Pleskot et al., 2012, 2013). The ability of PLDδ and its product, PA, to regulate microtubule cytoskeletal dynamics might contribute to plant resistance to non-host powdery mildew fungal penetration (Pinosa et al., 2013). AtPLDδ directly interacts with actin to modulate fundamental cellular processes (Angelayy et al., 2009), and our findings indicate that the protection of the actin cytoskeleton in self-incompatible pollen tubes by PbrPLDδ1 is mediated by its product, PA. The increased PA levels might slow the depolymerization of the actin cytoskeleton elicited by SI (Figure 8). However, our results show that PbrPLDδ1-derived PA is unable to reverse depolymerization of the actin cytoskeleton or to halt cell death in self-incompatible pollen tubes, pointing to the existence of other signaling pathways that terminate the growth of self-incompatible pollen tubes. Based on our data, we propose that PbrPLDδ1-derived PA plays a protective role in pear pollen tubes during the early stages of SI signaling, thus providing a connection between PLD/PA and SI. PLD/PA may be a key player in the recently proposed molecular mechanism described by the "all-or-nothing" or "S-RNase threshold phenomenon" hypothesis, which suggests that the SI response requires the presence of a minimum concentration of incompatible S-RNase in the pollen tube to ultimately trigger PCD (Soulard et al., 2014). Our findings are also consistent with the notion that PLDδ suppresses cell death in plants (Zhang et al., 2003; Li et al., 2004). Overall, our identification of the role of PbrPLDδ1 not only opens up a new avenue for studying S-RNase-based SI, but it also sheds light on the molecular nature of PLDδ-derived PA in response to biological stimuli.

In summary, we propose a model of a protective mechanism in pollen involving PbrS-RNase-mediated signaling during the early stages of the SI response. According to this model, a PbrS-RNase-induced increase in PA levels, as elicited by PbrPLDδ1

activity, initially hinders depolymerization of the actin cytoskeleton and protects pollen tubes against PCD (Figure 9). This pathway may be part of a protective "all-or-nothing" mechanism in pollen against PCD signaling that protect the pollen until sufficient incompatible PbrS-RNase activity ultimately triggers the induction of self-incompatible pollen tube death.

METHODS

Plant Materials

Pollen and styles were collected from two pear (*Pyrus bretschneideri*) cultivars with different *S*-genotypes: 'Dangshansuli' (S_7S_{34}) and 'Cuiguan' (S_3S_5). PbrS-RNase were extracted and purified from styles as previously described (Zhang and Hiratsuka, 2000). The concentration and activity of the PbrS-RNase extracts were determined as described previously (Brown and Ho, 1986).

Pollen Culture, SI Challenge, and Incubation in PA

'Dangshansuli' pollen was cultured in medium containing the following components: 5 mM MES, 440 mM sucrose, 0.55 mM $Ca(NO_3)_2$, 1.60 mM $MgSO_4$, 1.60 mM H_3BO_3, and 1.00 mM KNO_3, pH 6.5 (adjusted with Tris). 'Dangshansuli' stylar PbrS-RNase (S_7S_{34}) and 'Cuiguan' stylar PbrS-RNase (S_3S_5) were used as the incompatible and compatible treatments, respectively. The final concentration of PbrS-RNase used in the experiments was 0.15 units. After evaporating the chloroform solvent, PA was dissolved in culture medium and dispersed via 10 min of sonication in a water bath to form micelles. Pollen tubes were preincubated with 20 μM PA for 10 min before adding PbrS-RNase or 1-butanol.

$^{32}P_i$ PA Labeling, Extraction, and Analysis

A PA level dynamic assay was performed as described previously (Zonia and Munnik, 2004). At the start of culture, PA in pollen tubes was labeled with 200 μCi/mL carrier-free $^{32}PO_4^{3-}$ (Perkin-Elmer) for 4 h prior to treatment. The reaction was stopped by adding 50 μL 50% (v/v) perchloric acid to 450 μL pollen suspension and immediately freezing the sample in liquid nitrogen (N_2). After thawing, the samples were vortexed for 1 min and centrifuged at 9000*g* for 2 min, and the supernatant was removed. To extract the lipids in the supernatant, 750 μL $CHCl_3$:MeOH:HCl (50:100:1, v/v) was added, and the mixture was vortexed for 5 min prior to freezing again in liquid N_2. After thawing, the samples were immediately vortexed and centrifuged as before. Subsequently, 750 μL $CHCl_3$ and 200 μL 0.9% (w/v) NaCl were added to the samples, followed by vortexing and centrifugation. The aqueous upper phase was removed, and the organic lower phase was transferred to a new tube containing 750 μL $CHCl_3$:MeOH:1 N HCl (3:48:47; v/v). After vortexing and centrifuging, the upper phase was again discarded before adding 20 μL isopropanol. Finally, the lipid extracts were dried by vacuum centrifugation and dissolved in 20 μL $CHCl_3$.

Silica-60 thin-layer chromatography plates (Merck) were used to quantify lipid contents. To this end, an ethyl acetate-based solvent composed of ethyl acetate:iso-octane:formic acid: water (13:2:3:10; v/v) was used as the mobile phase during chromatography for PBut and PA. Since it is difficult to obtain pure, radiolabeled PA and PBut, radiolabeled phospholipids are often extracted from hyperosmotically stimulated *Chlamydomonas moewusii* or tobacco (*Nicotiana tabacum*) pollen tubes and used as standards (Zonia and Munnik, 2004). Thus, in this study, to indicate the exact positions of PA and PBut produced from pear pollen on the thin layer chromatography plate, we used radiolabeled lipids from tobacco pollen tubes as standards. Radioactivity was measured by autoradiography (X-Omat S; Eastman Kodak) and quantified by phosphor imaging (Storm; Molecular Dynamics). Plot analysis using ImageJ software was performed to quantify the ^{32}PA and ^{32}PBut contents in each sample. To compare ^{32}PA and ^{32}PBut values after perturbation, the experimental values were normalized to that of the control.

Identification and Phylogenetic Analysis of the *PLD* Gene Family in Pear

Genomic and publicly available annotated protein databases for pear (*P. bretschneideri*) were downloaded from the pear genome project (http://peargenome.njau.edu.cn/). Multiple strategies were used to search for members of the PLD family in pear. First, searches with the keyword "Phospholipase D" were performed against the annotated pear protein databases. Second, Hidden Markov Model searches (HMMsearch) with the HKD domain HMM profile (PF00614) for proteins with catalytic functions of PLD that are highly conserved in each plant species were conducted, and all significant hits (HMMER E value < e-5) were subsequently evaluated. Finally, *Arabidopsis thaliana* and rice (*Oryza sativa*) PLD protein sequences were used as queries in exhaustive BLAST searches with standard parameters until there was convergence with the pear protein data. All PLD protein sequences were again analyzed using the InterProScan5 database (http://www.ebi.ac.uk/interpro/search/sequence-search) to verify the presence of the HKD domain; protein sequences lacking this domain were removed. Pear PLDs were named based on the nomenclature established for the Arabidopsis and rice PLD families. The amino acid sequences of the selected PLDs were aligned with ClustalX, and the alignment is provided in Supplemental File 1. ProtTest was used to evaluate the best model of substitution to infer the optimal phylogeny. Phylogenetic trees were produced via the maximum likelihood method in MEGA6.1 using the best amino acid substitution model. Bootstrapping was performed with 1000 iterations using the parameters *p*-distance and partial deletion with 95% site coverage cutoff option.

RT-qPCR

RT-qPCR analysis was performed following Minimum Information for Publication of Quantitative Real-Time PCR Experiments (MIQE) guidelines (Bustin et al., 2009). Supplemental Table 1 shows the primers used in this study. Total RNA was extracted using the TRIzol reagent (Takara) according to the manufacturer's instructions. RNA quality was assessed according to OD 260/280 > 2.0, OD 260/230 > 1.8, and gel electrophoresis. Equal amounts of total RNA (2 μg) were treated with DNase I to eliminate genomic DNA contamination and used as templates for cDNA synthesis using a PrimeScript RT Reagent Kit (Perfect Real Time; Takara). To assess gDNA contamination, amplification of *PbrEF1α* using a primer that spanned an intron (Chen et al., 2015) was performed for all cDNA samples. Subsequently, 20 μL of the mixture, corresponding to 5 ng of total cDNA, was used per PCR (Takara SYBR PrimeScript RT-PCR Kit for Perfect Real Time) with a Roche LightCycler 480II system following the manufacturer's instructions. Lin-RegPCR was used to calculate the efficiency of the primers during RT-qPCR. The expression levels of *PLD* genes in all samples were determined based on their cycle threshold values.

as-ODN Silencing of *PbrPLD* Expression

The as-ODN experiment was performed as previously described (Pleskot et al., 2010). ODN sequences targeting *PbrPLD*s were designed using the RNA fold web serve (http://rna.tbi.univie.ac.at/cgi-bin/RNAWebSuite/RNAfold.cgi). Soligo software (http://sfold.wadsworth.org/cgi-bin/soligo.pl) was used to evaluate candidate as-ODN sequences for suitable target regions. The three candidate as-ODNs with the highest scores and their corresponding sense-ODNs (s-ODNs) for each *PLD* were synthesized using phosphorothioate and purified by high-performance liquid chromatography.

A premix of ODN/cytofectin complexes was incubated in cultivation medium for 15 min before adding the mixture to the pollen culture to a final concentration of 50 μM ODN. After the addition of 15 μg/mL ODN, the pollen was cultivated in this mixture for 4 h. The as-/s-ODN pairs were tested for their effect on the relative expression levels of target genes, and the most effective pair (marked #1 in Supplemental Table 1) was used for further analysis.

Evaluation of PCD in Pear Pollen Tubes

PCD was evaluated by TUNEL staining as described previously (Wang et al., 2009). After fixing the samples in 4% paraformaldehyde for 2 h, the pollen tubes were transferred to 70% ethanol for at least 4 h at –20°C. The samples were then washed with PBS (pH 7.4) and stained using the Dead End Fluorometric TUNEL system (Promega) per the manufacturer's instructions. After TUNEL staining, the samples were washed with citrate buffer (pH 4.1) and stained with 0.05 μg/mL 4′,6-diamidino-2-phenylindole (Sigma-Aldrich). Positive TUNEL staining in pollen tubes indicated PCD.

PbrS-RNase Point Mutants and the Y2H Assay

The full-length *PbrS-RNase* sequence (without the signal peptide) was introduced into the pMD 19-T vector (Takara). Point mutations were introduced into $PbrS_7$-RNase using a QuikChange site-directed mutagenesis kit (Stratagene). After the mutation was confirmed by sequencing, the mutagenic gene was transferred into the pGBKT7 vector for the Y2H assay. To confirm interactions between PbrPLDδ1, $PbrS_7$-RNase (without the signal peptide), $PbrS_{34}$-RNase (without the signal peptide), and PbrActin1, the full-length or truncated gene was cloned into the *Eco*RI and *Sal*I sites of the pGBKT7 vector or the *Eco*RI and *Xho*I sites of the pGADT7 vector (Supplemental Table 1). AH109 yeasts cells were cotransformed using the LiCl-PEG method and grown on selection plates with SD/–Leu–Trp (–W, –L) medium to select cotransformed cells and SD/–Trp–Leu–His–Ade (–W, –L, –H, –A) medium with 15 mM 3-AT to monitor protein interactions. BD-53 and AD-SV40 were used as positive controls and BD-Lam and AD-SV40 as negative controls. Positive interaction between PbrS-RNase and PbrActin1 was confirmed by a filter assay to detect 5-bromo-4-chloro-3-indolyl-β-D-galactopyranoside acid (X-gal) (80 μg/mL) activity. The interaction strength was quantified based on β-galactosidase activity using *o*-nitrophenyl-β-D-galactopyranoside as the substrate. The precise protocols were provided by Clontech Laboratories.

Production of $PbrS_7$-RNase Recombinant Proteins in *Escherichia coli*

The DNA sequence corresponding to $PbrS_7$-RNase was amplified by PCR and inserted into the pCold-TF expression vector to create His-tagged recombinant $PbrS_7$-RNase protein. The Trigger Factor (TF) chaperone in this vector is used as a soluble tag; the molecular weight of TF-His tag is ~48 kD. Protein expression was induced in *E. coli Rosetta* (DE3) cells. Recombinant *E. coli* cells were incubated at 37°C overnight in the presence of the appropriate antibiotics, each diluted 1:30 in LB medium (10 mL overnight culture solution added to 290 mL LB medium). The culture was allowed to grow for an additional 1 to 3 h at 37°C with shaking at 200 rpm. When the OD_{600} of the culture reached 0.4 to 0.8, the culture was quickly cooled to 15°C in ice water and incubated for 30 min. After the addition of 0.5 mM isopropyl-β-D-thiogalactosidase (Sigma-Aldrich), the culture solution was incubated with shaking at 15°C for 24 h to allow the recombinant protein to be expressed. The culture was transferred to a falcon tube and centrifuged at 12,000*g* for 15 min to harvest the cells. The cells were incubated in a rotary device at room temperature for 20 min and sonicated on ice (3 × 5 s), with a 30-s rest between each pulse to allow for cooling. The cell lysate was centrifuged (12,000 rpm, 15 min) at 4°C, and the supernatant was transferred to a fresh tube. Protein loading dye (5×) was added to each sample before analysis by SDS-PAGE.

To purify the $PbrS_7$-RNase recombinant protein from *E. coli*, the supernatant containing soluble protein was loaded onto a column containing 2 mL Ni-NTA His Bind resin (Novagen) and washed with 30 mL binding buffer (500 mM NaCl, 20 mM Tris-HCl, and 5 mM imidazole, pH 7.9) and 40 mL wash buffer (500 mM NaCl, 40 mM imidazole, and 20 mM Tris-HCl, pH 7.9) prior to elution with 40 mL elution buffer (70 mM imidazole, 500 mM NaCl, and 20 mM Tris-HCl, pH 7.9). The eluate was dialyzed (Spectra/por membrane molecular cutoff 50 kD) against dialysis buffer (25 mM Tris-HCl, pH 8.0) at 4°C for 16 h.

Site substitution mutants of $PbrS_7$-RNase (116H/116R, 149L/149A, 154I/154A, and 156P/156A) and $PbrS_{34}$-RNase (116H/116R, 149L/149A, 154I/154A, and 156P/156A) were constructed using the Fast Mutagenesis System (TransGen Biotech). Mutagenic primers were designed according to the manufacturer's instructions using GenBank sequences for $PbrS_7$-RNase (*P. bretschneideri* S_7-RNase; AB002143.1) and $PbrS_{34}$-RNase (*P. bretschneideri* S_{34}-RNase; DQ414813.1). The primers used are shown in Supplemental Table 1.

Crystal Structure Graphics

Protein Data Bank entries for RNase T2 proteins (Matsuura et al., 2001; Gundampati et al., 2012; Thorn et al., 2012) were downloaded from the RCSB Protein Data Bank (http://www.rcsb.org/pdb/home/home.do). Graphical models of the structures of these proteins were produced with the PyMOL program (PyMOL molecule rendering; https://pymol.org) (Mura et al., 2010).

Calculation of the Equilibrium Dissociation Constant (K_d)

Using recombinant PbrS-RNases, K_d for the binding of PbrS-RNase to F-actin was estimated via cosedimentation reactions with 0.5 μM (corresponding to 15 μg/mL) $PbrS_7$-RNase and increasing concentrations of phalloidin-stabilized F-actin according to a previous report (Khurana et al., 2010). Following high-speed centrifugation, the percentage of S_7-RNase in the pellet was determined by densitometry. The data were plotted as a function of the actin concentration and fitted with a hyperbolic function to estimate K_d values using KaleidaGraph v3.6 software (Synergy Software).

Depolymerization Assays and Quantification of Filamentous Actin Levels in Vivo

An F-actin depolymerization assay was conducted and the amount of F-actin present in the samples was quantified as previously described (Huang et al., 2006). After each reaction, the pollen samples were stabilized in 200 μM MES-buffered saline and fixed in 4% paraformaldehyde. The samples were then stained individually with 5 μM rhodamine-phalloidin for the depolymerization assay or simultaneously with 5 μM rhodamine-phalloidin and 5 μM ethidium bromide (EB) for the quantification assay. A Zeiss LSM700 confocal microscope was used to examine the levels of actin depolymerization, and phalloidin fluorescence divided by EB fluorescence was used as an index for actin filament levels. The bound phalloidin and EB were eluted with methanol and quantified by spectrofluorometry with excitation and emission wavelengths of 492 and 514 nm, respectively, for phalloidin and 513 and 615 nm, respectively, for EB.

Dynamic Depolymerization Assay and Microscopy Detection of Actin Filaments in Vitro

A dynamic depolymerization assay and microscopy detection of actin filaments in vitro were conducted as previously reported (Huang et al., 2006). F-actin at 0.5 mM (50% pyrene-labeled) was mixed with different concentrations of PbrS-RNase for 5 min and diluted 50-fold in a polymerization solution of 1× KMEI (500 mM KCl, 10 mM $MgCl_2$, 10 mM EGTA, and 100 mM imidazole-HCl, pH 7.0) at room temperature. The decrease in pyrene fluorescence concomitant with actin depolymerization was monitored for 60 min after dilution. After being assembled from 0.5 mM G-actin for 60 min, preformed

F-actin was incubated with PbrS-RNase in 1× KMEI for different times and stained with 0.5 mM rhodamine-phalloidin for an additional 15 min. The F-actin was the diluted 25-fold in fluorescence buffer containing 1 mM $MgCl_2$, 50 mM KCl, 100 mM DTT, 10 mM imidazole, 0.5% methylcellulose, 20 μg/mL catalase, 15 mg/mL glucose, and 100 μg/mL glucose oxidase at pH 7.0 and transferred to a cover slip coated with poly-L-lysine (0.01%) for observation under a Zeiss LSM700 laser confocal microscope with a 100×/1.45 oil objective.

TIRF Microscopy

The actin filament-severing assays were performed using a previously described procedure, with minor modifications (Chaudhry et al., 2013). Preformed F-actin (polymerized from 0.5 mM rhodamine-labeled G-actin) was equilibrated in 1× TIRF buffer (1 mM $MgCl_2$, 50 mM KCl, 0.2 mM ATP, 1 mM EGTA, 10 mM DTT, 10 mM imidazole, 15 mM glucose, 20 μg/mL catalase, 0.5% methylcellulose, and 100 μg/mL glucose oxidase, pH 7.4) and added to a flow cell coated with myosin. After ~4 min, the reaction mixture was replaced with 1× TIRF buffer containing 0.15 units of PbrS-RNase by wicking. The samples were observed by spinning-disc confocal microscopy (Yokogawa Electric) with a 100×/1.45 oil objective. Time-lapse images were collected every 60 s for 600 s by TIRF microscopy. The average severing frequency was surveyed using ImageJ.

Statistical Analysis

All experimental data are the averages of at least three independent replicates and are shown as the mean ± SE. The data were analyzed using SPSS software, and statistical differences were compared based on Student's *t* test for two groups of samples and ANOVA for multiple samples. ANOVA tables are provided in Supplemental Data Set 1. For multiple comparisons, Tukey's honestly significant difference test was performed.

Accession Numbers

The complete sequences of *PbrPLDδ1* and *PbrActin1* have been deposited in the GenBank data libraries under accession numbers KY694375 and KY694376, respectively.

Supplemental Data

Supplemental Figure 1. PbrS-RNase interacts with the actin cytoskeleton during the SI response.

Supplemental Figure 2. Structural analysis of four RNase proteins.

Supplemental Figure 3. Recombinant PbrS-RNases have inhibitory effects on incompatible pollen.

Supplemental Figure 4. Mutation in the actin binding domain does not affect the RNase activity of $PbrS_{34}$-RNase.

Supplemental Figure 5. TIRF microscopy analysis of actin filament depolymerization by PbrS-RNase P156A.

Supplemental Figure 6. Sequence alignment of $PbrS_7$-RNase, $PbrS_{34}$-RNase, and petunia S_3-RNase.

Supplemental Figure 7. Effect of PLD-PA on pear pollen germination and tube growth.

Supplemental Figure 8. Identification, phylogenetic analysis, and domain analyses of pear *PLD* genes.

Supplemental Figure 9. PbrPLDδ1 is localized to the plasma membrane.

Supplemental Figure 10. PCR analysis of *PbrPLD* expression in ODN-mediated knockdown lines.

Supplemental Figure 11. Knockdown of *PbrPLDδ1* increases SI-induced pollen tube death rates based on FDA analysis.

Supplemental Figure 12. Identification of the PA concentration required to mitigate the effects of PbrS-RNase plus 1-butanol treatment in incompatible pollen tubes.

Supplemental Figure 13. Quantification of actin cytoskeleton depolymerization in pollen tubes after various treatments.

Supplemental Figure 14. Y2H analysis of the interaction between PbrPLDδ1 and PbrS-RNase.

Supplemental Table 1. Primers used in this study.

Supplemental Data Set 1. ANOVA tables.

Supplemental File 1. Text file corresponding to the alignment used for phylogenetic analysis in Supplemental Figure 8.

ACKNOWLEDGMENTS

We thank Suomeng Dong for his important insights into the plant immune system. This work was supported by the grants from National Natural Science Foundation of China (31522048, 31501715, 31772256, and 31772276), the National Key Technology R&D Program of the Ministry of Science and Technology of China (2014BAD16B03-4), the National Natural Science Foundation of Jiangsu Province (BK20150676), Fundamental Research Funds for the Central Universities (KYTZ201602 and KYLH201502-2), and Research Funds for the Universities of Fujian Province of China (JK2017017).

AUTHOR CONTRIBUTIONS

J.W. and S.Z. initiated and supervised the project. J.C. and J.W. conceived the experiments and wrote the manuscript. P.W., S.Z., and B.H.J.d.G critically read and commented on the manuscript. J.C., P.W., H.Z., C.T., and H.J. performed the experiments. All of the authors were involved in data analysis and interpretation.

Received January 9, 2018; revised April 9, 2018; accepted April 27, 2018; published April 30, 2018.

REFERENCES

Anderson, M.A., et al. (1986). Cloning of cDNA for a stylar glycoprotein associated with expression of self-incompatibility in *Nicotiana alata.* Nature **321:** 38–44.

Angelayy, H., Davida, D., Melissah, B., and Jan, M. (2009). Arabidopsis phospholipase Dδ as an initiator of cytoskeleton-mediated signalling to fundamental cellular processes. Funct. Plant Biol. **36:** 190–198.

Boivin, N., Morse, D., and Cappadocia, M. (2014). Degradation of S-RNase in compatible pollen tubes of *Solanum chacoense* inferred by immunogold labeling. J. Cell Sci. **127:** 4123–4127.

Brown, P.H., and Ho, T.-H.D. (1986). Barley aleurone layers secrete a nuclease in response to gibberellic acid: purification and partial characterization of the associated ribonuclease, deoxyribonuclease, and 3′-nucleotidase activities. Plant Physiol. **82:** 801–806.

Bustin, S.A., Benes, V., Garson, J.A., Hellemans, J., Huggett, J., Kubista, M., Mueller, R., Nolan, T., Pfaffl, M.W., Shipley, G.L., Vandesompele, J., and Wittwer, C.T. (2009). The MIQE guidelines: minimum information for publication of quantitative real-time PCR experiments. Clin. Chem. **55:** 611–622.

Chaudhry, F., Breitsprecher, D., Little, K., Sharov, G., Sokolova, O., and Goode, B.L. (2013). Srv2/cyclase-associated protein forms hexameric shurikens that directly catalyze actin filament severing by cofilin. Mol. Biol. Cell **24:** 31–41.

Chen, J., Li, X., Wang, D., Li, L., Zhou, H., Liu, Z., Wu, J., Wang, P., Jiang, X., Fabrice, M.R., Zhang, S., and Wu, J. (2015). Identification and testing of reference genes for gene expression analysis in pollen of *Pyrus bretschneideri.* Sci. Hortic. (Amsterdam) **190:** 43–56.

de Graaf, B.H., Rudd, J.J., Wheeler, M.J., Perry, R.M., Bell, E.M., Osman, K., Franklin, F.C.H., and Franklin-Tong, V.E. (2006). Self-incompatibility in *Papaver* targets soluble inorganic pyrophosphatases in pollen. Nature **444:** 490–493.

De Nettancourt, D. (2001). Incompatibility and Incongruity in Wild and Cultivated Plants. (Berlin: Springer).

Doucet, J., Lee, H.K., and Goring, D.R. (2016). Pollen acceptance or rejection: a tale of two pathways. Trends Plant Sci. **21:** 1058–1067.

Eliás, M., Potocký, M., Cvrcková, F., and Zárský, V. (2002). Molecular diversity of phospholipase D in angiosperms. BMC Genomics **3:** 2.

Estruch, J.J., Kadwell, S., Merlin, E., and Crossland, L. (1994). Cloning and characterization of a maize pollen-specific calcium-dependent calmodulin-independent protein kinase. Proc. Natl. Acad. Sci. USA **91:** 8837–8841.

Franklin-Tong, V.E. (2008). Self-Incompatibility in Flowering Plants: Evolution, Diversity, and Mechanisms. (Berlin: Springer).

Franklin-Tong, V.E., and Gourlay, C.W. (2008). A role for actin in regulating apoptosis/programmed cell death: evidence spanning yeast, plants and animals. Biochem. J. **413:** 389–404.

Fujii, S., Kubo, K., and Takayama, S. (2016). Non-self- and self-recognition models in plant self-incompatibility. Nat. Plants **2:** 16130.

Gardiner, J., Collings, D.A., Harper, J.D., and Marc, J. (2003). The effects of the phospholipase D-antagonist 1-butanol on seedling development and microtubule organisation in Arabidopsis. Plant Cell Physiol. **44:** 687–696.

Goldraij, A., Kondo, K., Lee, C.B., Hancock, C.N., Sivaguru, M., Vazquez-Santana, S., Kim, S., Phillips, T.E., Cruz-Garcia, F., and McClure, B. (2006). Compartmentalization of S-RNase and HT-B degradation in self-incompatible *Nicotiana.* Nature **439:** 805–810.

Gray, J.E., McClure, B.A., Bonig, I., Anderson, M.A., and Clarke, A.E. (1991). Action of the style product of the self-incompatibility gene of *Nicotiana alata* (S-RNase) on *in vitro*-grown pollen tubes. Plant Cell **3:** 271–283.

Gundampati, R.K., Chikati, R., Kumari, M., Sharma, A., Pratyush, D.D., Jagannadham, M.V., Kumar, C.S., and Debnath Das, M. (2012). Protein-protein docking on molecular models of *Aspergillus niger* RNase and human actin: novel target for anticancer therapeutics. J. Mol. Model. **18:** 653–662.

Helling, D., Possart, A., Cottier, S., Klahre, U., and Kost, B. (2006). Pollen tube tip growth depends on plasma membrane polarization mediated by tobacco PLC3 activity and endocytic membrane recycling. Plant Cell **18:** 3519–3534.

Higashiyama, T., and Takeuchi, H. (2015). The mechanism and key molecules involved in pollen tube guidance. Annu. Rev. Plant Biol. **66:** 393–413.

Huang, S., Lee, H.S., Karunanandaa, B., and Kao, T.H. (1994). Ribonuclease activity of *Petunia inflata* S proteins is essential for rejection of self-pollen. Plant Cell **6:** 1021–1028.

Huang, S., Gao, L., Blanchoin, L., and Staiger, C.J. (2006). Heterodimeric capping protein from *Arabidopsis* is regulated by phosphatidic acid. Mol. Biol. Cell **17:** 1946–1958.

Jones, J.D.G., and Dangl, J.L. (2006). The plant immune system. Nature **444:** 323–329.

Khurana, P., Henty, J.L., Huang, S., Staiger, A.M., Blanchoin, L., and Staiger, C.J. (2010). Arabidopsis VILLIN1 and VILLIN3 have overlapping and distinct activities in actin bundle formation and turnover. Plant Cell **22:** 2727–2748.

Kumar, A., and McClure, B. (2010). Pollen-pistil interactions and the endomembrane system. J. Exp. Bot. **61:** 2001–2013.

Lai, Z., Ma, W., Han, B., Liang, L., Zhang, Y., Hong, G., and Xue, Y. (2002). An F-box gene linked to the self-incompatibility (*S*) locus of *Antirrhinum* is expressed specifically in pollen and tapetum. Plant Mol. Biol. **50:** 29–42.

Li, G., Lin, F., and Xue, H.-W. (2007). Genome-wide analysis of the phospholipase D family in *Oryza sativa* and functional characterization of PLD β 1 in seed germination. Cell Res. **17:** 881–894.

Li, J., Henty-Ridilla, J.L., Huang, S., Wang, X., Blanchoin, L., and Staiger, C.J. (2012). Capping protein modulates the dynamic behavior of actin filaments in response to phosphatidic acid in *Arabidopsis.* Plant Cell **24:** 3742–3754.

Li, J., Henty-Ridilla, J.L., Staiger, B.H., Day, B., and Staiger, C.J. (2015). Capping protein integrates multiple MAMP signalling pathways to modulate actin dynamics during plant innate immunity. Nat. Commun. **6:** 7206.

Li, W., Li, M., Zhang, W., Welti, R., and Wang, X. (2004). The plasma membrane-bound phospholipase Ddelta enhances freezing tolerance in *Arabidopsis thaliana*. Nat. Biotechnol. **22:** 427–433.

Liu, Z.Q., Xu, G.H., and Zhang, S.L. (2007). *Pyrus pyrifolia* stylar S-RNase induces alterations in the actin cytoskeleton in self-pollen and tubes *in vitro.* Protoplasma **232:** 61–67.

Luhtala, N., and Parker, R. (2010). T2 Family ribonucleases: ancient enzymes with diverse roles. Trends Biochem. Sci. **35:** 253–259.

Luu, D.T., Qin, X., Morse, D., and Cappadocia, M. (2000). S-RNase uptake by compatible pollen tubes in gametophytic self-incompatibility. Nature **407:** 649–651.

Matsumoto, D., and Tao, R. (2012). Isolation of pollen-expressed actin as a candidate protein interacting with S-RNase in *Prunus avium* L. J. Jpn. Soc. Hortic. Sci. **81:** 41–47.

Matsuura, T., Sakai, H., Unno, M., Ida, K., Sato, M., Sakiyama, F., and Norioka, S. (2001). Crystal structure at 1.5-A resolution of *Pyrus pyrifolia* pistil ribonuclease responsible for gametophytic self-incompatibility. J. Biol. Chem. **276:** 45261–45269.

McCubbin, A.G., Chung, Y.Y., and Kao, T. (1997). A mutant S_3-RNase of *Petunia inflata* lacking RNase activity has an allele-specific dominant negative effect on self-incompatibility interactions. Plant Cell **9:** 85–95.

Meng, D., Gu, Z., Li, W., Wang, A., Yuan, H., Yang, Q., and Li, T. (2014). Apple MdABCF assists in the transportation of S-RNase into pollen tubes. Plant J. **78:** 990–1002.

Monteiro, D., Liu, Q., Lisboa, S., Scherer, G.E.F., Quader, H., and Malhó, R. (2005). Phosphoinositides and phosphatidic acid regulate pollen tube growth and reorientation through modulation of $[Ca^{2+}]_c$ and membrane secretion. J. Exp. Bot. **56:** 1665–1674.

Moutinho, A., Camacho, L., Haley, A., Pais, M.S., Trewavas, A., and Malhó, R. (2001). Antisense perturbation of protein function in living pollen tubes. Sex. Plant Reprod. **14:** 101–104.

Munnik, T. (2001). Phosphatidic acid: an emerging plant lipid second messenger. Trends Plant Sci. **6:** 227–233.

Mura, C., McCrimmon, C.M., Vertrees, J., and Sawaya, M.R. (2010). An introduction to biomolecular graphics. PLOS Comput. Biol. **6:** e1000918.

Nesiel-Nuttman, L., Doron, S., Schwartz, B., and Shoseyov, O. (2014). Human RNASET2 derivatives as potential anti-angiogenic agents: actin binding sequence identification and characterization. Oncoscience **2:** 31–43.

Pinosa, F., Buhot, N., Kwaaitaal, M., Fahlberg, P., Thordal-Christensen, H., Ellerström, M., and Andersson, M.X. (2013). Arabidopsis phospholipase dδ is involved in basal defense and nonhost resistance to powdery mildew fungi. Plant Physiol. **163:** 896–906.

Pleskot, R., Potocký, M., Pejchar, P., Linek, J., Bezvoda, R., Martinec, J., Valentová, O., Novotná, Z., and Zárský, V. (2010). Mutual regulation of plant phospholipase D and the actin cytoskeleton. Plant J. **62:** 494–507.

Pleskot, R., Pejchar, P., Bezvoda, R., Lichtscheidl, I.K., Wolters-Arts, M., Marc, J., Zárský, V., and Potocký, M. (2012). Turnover of phosphatidic acid through distinct signaling pathways affects multiple aspects of pollen tube growth in tobacco. Front. Plant Sci. **3:** 54.

Pleskot, R., Li, J., Zárský, V., Potocký, M., and Staiger, C.J. (2013). Regulation of cytoskeletal dynamics by phospholipase D and phosphatidic acid. Trends Plant Sci. **18:** 496–504.

Qiao, H., Wang, F., Zhao, L., Zhou, J., Lai, Z., Zhang, Y., Robbins, T.P., and Xue, Y. (2004). The F-box protein AhSLF-S_2 controls the pollen function of S-RNase-based self-incompatibility. Plant Cell **16:** 2307–2322.

Qin, C., and Wang, X. (2002). The Arabidopsis phospholipase D family. Characterization of a calcium-independent and phosphatidylcholine-selective PLD ζ 1 with distinct regulatory domains. Plant Physiol. **128:** 1057–1068.

Roiz, L., Smirnoff, P., Bar-Eli, M., Schwartz, B., and Shoseyov, O. (2006). ACTIBIND, an actin-binding fungal T_2-RNase with antiangiogenic and anticarcinogenic characteristics. Cancer **106:** 2295–2308.

Sanabria, N., Goring, D., Nürnberger, T., and Dubery, I. (2008). Self/nonself perception and recognition mechanisms in plants: a comparison of self-incompatibility and innate immunity. New Phytol. **178:** 503–514.

Sassa, H., Hirano, H., and Ikehashi, H. (1992). Self-incompatibility-related RNases in styles of Japanese pear (*Pyrus Serotina* Rehd). Plant Cell Physiol. **33:** 811–814.

Sijacic, P., Wang, X., Skirpan, A.L., Wang, Y., Dowd, P.E., McCubbin, A.G., Huang, S., and Kao, T.H. (2004). Identification of the pollen determinant of S-RNase-mediated self-incompatibility. Nature **429:** 302–305.

Soulard, J., Boivin, N., Morse, D., and Cappadocia, M. (2014). eEF1A is an S-RNase binding factor in self-incompatible *Solanum chacoense.* PLoS One **9:** e90206.

Thomas, S.G., Huang, S., Li, S., Staiger, C.J., and Franklin-Tong, V.E. (2006). Actin depolymerization is sufficient to induce programmed cell death in self-incompatible pollen. J. Cell Biol. **174:** 221–229.

Thorn, A., Steinfeld, R., Ziegenbein, M., Grapp, M., Hsiao, H.H., Urlaub, H., Sheldrick, G.M., Gärtner, J., and Krätzner, R. (2012). Structure and activity of the only human RNase T2. Nucleic Acids Res. **40:** 8733–8742.

Wang, X. (2002). Phospholipase D in hormonal and stress signaling. Curr. Opin. Plant Biol. **5:** 408–414.

Wang, C.L., Xu, G.H., Jiang, X.T., Chen, G., Wu, J., Wu, H.Q., and Zhang, S.L. (2009). S-RNase triggers mitochondrial alteration and DNA degradation in the incompatible pollen tube of *Pyrus pyrifolia* in vitro. Plant J. **57:** 220–229.

Wang, C.L., Wu, J., Xu, G.H., Gao, Y.B., Chen, G., Wu, J.Y., Wu, H.Q., and Zhang, S.L. (2010). S-RNase disrupts tip-localized reactive oxygen species and induces nuclear DNA degradation in incompatible pollen tubes of *Pyrus pyrifolia.* J. Cell Sci. **123:** 4301–4309.

Wu, J., et al. (2013). The genome of the pear (*Pyrus bretschneideri* Rehd.). Genome Res. **23:** 396–408.

Xue, Y., Carpenter, R., Dickinson, H.G., and Coen, E.S. (1996). Origin of allelic diversity in antirrhinum *S* locus RNases. Plant Cell **8:** 805–814.

Yanagisawa, M., Desyatova, A.S., Belteton, S.A., Mallery, E.L., Turner, J.A., and Szymanski, D.B. (2015). Patterning mechanisms of cytoskeletal and cell wall systems during leaf trichome morphogenesis. Nat. Plants **1:** 15014.

Zhang, S., and Hiratsuka, S. (2000). Effects of the stylar S-glycoproteins on the pollen germination and the tube growth in pears (*Pyrus serotina* Rhed.) in vitro. Yuan Yi Xue Bao **27:** 251–256.

Zhang, W., Wang, C., Qin, C., Wood, T., Olafsdottir, G., Welti, R., and Wang, X. (2003). The oleate-stimulated phospholipase D, PLDdelta, and phosphatidic acid decrease H2O2-induced cell death in Arabidopsis. Plant Cell **15:** 2285–2295.

Zonia, L., and Munnik, T. (2004). Osmotically induced cell swelling versus cell shrinking elicits specific changes in phospholipid signals in tobacco pollen tubes. Plant Physiol. **134:** 813–823.